Annals of Nuclear Energy 184 (2023) 109672

Contents lists available at ScienceDirect

Annals of Nuclear Energy

journal homepage: www.elsevier.com/locate/anucene

Assessing water-wall behaviour for a light-water Small Modular Reactor with the aid of CFD analyses

Alessandro De Angelis [a,*], Nils Reinke [b], Walter Ambrosini [a]

[a] Università di Pisa, Dipartimento di Ingegneria Civile e Industriale, Largo Lucio Lazzarino 2, 56122 Pisa, Italy
[b] Gesellschaft für Anlagen - und Reaktorsicherheit (GRS) gGmbH, Schwertnergasse 1, D-50667 Köln, Germany

ARTICLE INFO

Keywords:
Small Modular Reactors
Passive cooling
Water-wall
Containment
CFD

ABSTRACT

The paper summarises the results of a work performed in the frame of the EU ELSMOR project in the aim to characterise the behaviour of a reference Small Modular Reactor equipped with a passive containment system cooled by a surrounding water-wall. The work started with a review of the available literature, aimed at identifying experimental data possibly in a suitable scaling range, useful to draw conclusions about the decay heat rejection capabilities of such systems at full scale. This search for suitable data encountered difficulties, since the downscaling in height of most of the existing experimental facilities does not allow for reaching the target Rayleigh numbers envisaged for free convection in full scale reactor conditions (Ra $\sim 10^{16}$). In the lack of sufficient experimental information, it was firstly tried to reproduce downscaled experimental data by CFD; then, CFD was used to predict the water-wall behaviour in full scale configurations, on the basis of parametric assumptions about size and boundary conditions. The results help in sketching the phenomena that can be expected in reactor conditions at full scale, providing inter alia suggestions about pool mixing and the time needed to reach bulk boiling conditions. 2D, 3D and lumped parameter models were adopted using a range of assumptions to assess relevant phenomena. A study of the effect of geometrically downscaling facilities was also performed by CFD analyses. The obtained predictions of the system behaviour with different scales and assumptions address the present knowledge gap and are useful to highlight relevant phenomena on which experimental activities should be focused in the future.

1. Introduction

Small Modular Reactors (SMRs) are being considered for early deployment in the present decade as an advanced nuclear technology capable of further promoting the use of nuclear fission in a complementary segment of the energy market with respect to the one of large-scale reactor plants (see, e.g., IAEA, 2020).

Indeed, the use of nuclear fission is envisaged in the future energy mix in Europe and abroad to provide the stable source necessary to compensate for the high degree of intermittency of renewables in a decarbonised scenario. In particular, the European Commission, in the communication "A Clean planet for all" of November 2018 (European Commission, 2018) suggested that about 15 % of electricity produced by nuclear fission will form, together with Renewable Energy Sources (RES), the backbone of a decarbonised energy system in Europe in 2050. While the share of 15 % of nuclear electricity can be considered too low in front of the present 25 % and of the projections of increasing the electricity production owing to the electrification of several key sectors, the need to speed up in this process of decarbonisation is generally agreed at the political level worldwide. However, the target dates for reaching a net-zero carbon emission system may vary in the planning of different countries in the world.

Though the large size nuclear power plants remain the better assessed technology to be deployed for massive production of nuclear electricity, SMRs are presently considered by a large number of countries as a new generation of nuclear reactors with potential advantages in specific applications. In particular, as mentioned in IAEA (2020), SMRs have a number of advantageous features. In fact, it can be forecasted that reactors with a power up to 300 MWe may be more easily designed and built for early deployment in a modular fashion, which would compensate for the longer times needed to build large reactors. Moreover, their possible construction in workshops with production in series may abate costs and provide a flexible strategy for deployment of nuclear power to meet the needs of the decarbonisation process. For

* Corresponding author.
E-mail addresses: alessandro.deangelis@phd.unipi.it (A. De Angelis), Nils.Reinke@grs.de (N. Reinke), walter.ambrosini@unipi.it (W. Ambrosini).

https://doi.org/10.1016/j.anucene.2022.109672
Received 30 September 2022; Received in revised form 6 December 2022; Accepted 21 December 2022
Available online 9 January 2023

Table 1
Geometry quantities of the experimental apparatus used by Liu et al. (2018).

Parameter	Real Units	Scaled Units
Vessel height	19.8 m	1.02 m
Vessel diameter	4.4 m	0.219 m
Pool height	–	1.25 m
Pool square-base length side	–	0.5 m

instance, replacement of aged fossil fuelled plants by SMRs would constitute a smart way of preserving a distributed energy production while attaining the goals of decarbonisation, aiming to avoid or mitigate climate changes. Further advantages in the use of SMRs can be envisaged in their flexibility, especially for countries with small electricity grids or for electrification of remote areas. Hybrid systems involving SMRs interfaced with RES are also considered as a promising way of establishing a complementarity between more and less stable low-carbon energy sources in supporting decarbonisation. This complementarity needs interfacing baseload nuclear systems with the variable and intermittent production characterising solar and wind powers.

On the licensing side, any new nuclear reactor plant proposal must be anyway subjected to an attentive process of screening about safety. Issues to be specifically addressed for SMRs in this context (see again IAEA, 2020) are the management of multiple units by control room operators, the definition of the possible releases of radioactive material (i.e., the "source term") from multiple small units in view of emergency management and the definition of the surrounding zone to be considered potentially affected by an accident. The new aspects of load following capabilities related to the interfaces with intermittent renewable sources and the development of specific codes and standards for the new plant configurations are other issues to be considered. By the way, despite of the uncertainties intrinsic in any new technology, advantages are expected by the use of SMRs, as for instance a massive use of passivity, enabled by the low power, which would make possible to strongly decrease the probability of substantial emergencies since the design phase.

The ELSMOR (Towards European Licencing of Small Modular Reactors) Project *"seeks to design methods and tools for stakeholders to assess and verify LW-SMRs' safety when installed across Europe"* (see ELSMOR Project Website, i.e., ELSMOR, 2020). In this aim, a specific target is to collect and disseminate data on light-water Small Modular Reactors (LW-SMRs) safety issues, with reference to the European scenario. By setting up procedures for safety evaluation and enhancing the European infrastructure in support to the development and assessment of nuclear safety codes, the project will contribute to ease the licensing of future SMRs proposed, basing on light water-cooled nuclear reactor concepts. Work Package 4 of the project aims at developing and assessing analysis methods and tools for the safety demonstration of innovative containment safety functions characteristics. In this frame, a review of the state-of-the-art on available experimental data and an exercise for code assessment and development were organised, in whose frame the present work has been carried out.

In this paper, after a brief literature review of available experimental data that may be useful to support the analysis of a French SMR (F-SMR) containment design, the results of 2D and 3D CFD analyses, performed in support to project activities, are discussed to analyse the behaviour of a particular configuration of the containment decay heat removal system, equipped with a water-wall concept. CFD analyses were firstly performed for predicting the experimental data collected by an existing experimental facility, in order to consider the accuracy that could be obtained by the adopted tools; then, the CFD model was used to assess phenomena in full-scale conditions, also considering the possible differences that could be obtained at intermediate scaling. The obtained results help in sketching the possible flow and temperature patterns that can be envisaged to occur in the water pool facing the containment surface in real reactor conditions, also considering the applicability of information obtained by smaller scale facilities to the full-scale reactor size.

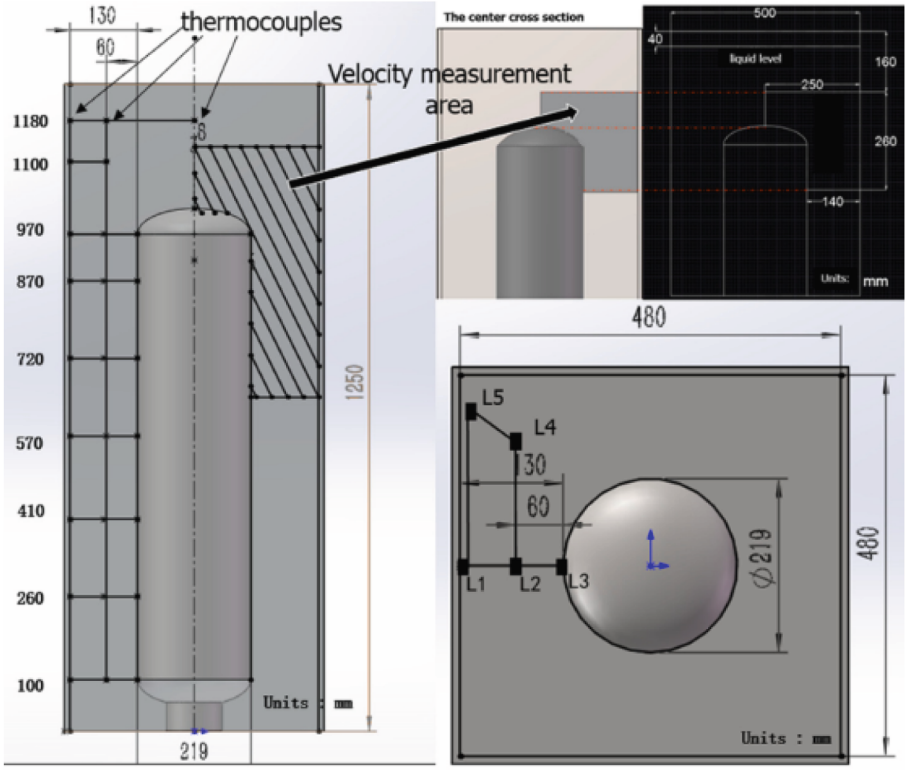

Fig. 1. Sketches of the experimental apparatus used by Liu et al. (2018) indicating the location of measurement devices.

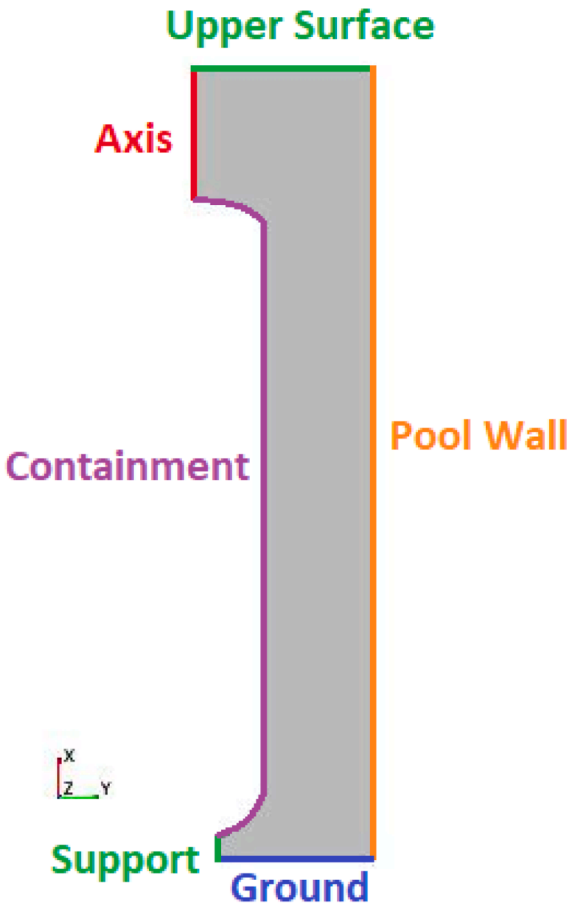

Fig. 2. Adopted geometry for CFD analyses with the related boundaries.

2. Literature survey about applicable experimental data

Subtask 4.2 of the ELSMOR project concerns the search for reliable experimental data that can be adopted for the validation of the codes that will be used to analyse and assess the passive cooling of the addressed SMR external containment.

As a matter of fact, besides the classical safety systems used in nowadays PWRs for controlling and mitigating the consequences of an accident scenario (e.g., the containment spray system and the various active residual heat removal systems), many SMR concepts are based on passive cooling systems for removing the decay heat during a Station Black Out (SBO) event or during a loss of coolant accident (LOCA) (IAEA, 2020). In particular, if a LOCA occurs in the primary cooling loop, the containment envelope will be filled with the steam generated at the leak and in some conceptual designs will be condensed onto the inner surface of the containment wall, which is cooled on the outer surface by a surrounding water pool, having the function of a large capacity heat sink. For this reason, the phenomena involved in the cooling process, as condensation of the steam in the presence of non-condensable gases and the flow and temperature fields in the water pool, need to be carefully investigated and quantified, aiming to reach the ultimate goal of proving the inherent safety of this type of SMRs. As mentioned in the introduction, this is finally aimed to establish a licensing methodology for these units, something that is of high relevance for the future low-carbon energy mix in Europe, to be based on nuclear and renewable energy sources, among which SMRs are presently considered to play a relevant role.

To date, it is still difficult to find specific experimental data suitable for a full-scale validation of models for the prediction of relevant phenomena of interest for SMR passive systems in the water pools. The large values of some geometrical parameters (e.g., the height of the external containment vessel) lead to high values of the dimensionless numbers directly involved in natural convection conditions, such as the Rayleigh number, directly proportional to the cube of the height of the system. Owing to the high values of these dimensionless parameters (the Rayleigh number has to be in the order of 10^{16}), pretty hard to achieve during experimental campaigns which are not made on full-scale facilities, it is difficult to find reliable experimental data and heat transfer correlations which can be safely used to be included in system thermal–hydraulic codes conceived for safety analyses. The experimental data that can be found in literature mostly derive from experimental campaigns made on downscaled units, e.g., addressing water-wall heat transfer phenomena driven by natural convection in small apparatuses, useful for a preliminary validation of thermal–hydraulic codes.

Liu et al. (2018) and Albadawi et al. (2018) carried out experimental campaigns on a downscaled unit of the NuScale Small Modular Reactor (see, e.g., IAEA, 2020) achieving interesting results about the temperature behaviour and velocity fields in the water-wall (i.e., in the cooling pool) with different levels of thermal power released in the containment. Moreover, in the same works, a CFD model was adopted to simulate the achieved experimental data; in this frame, Liu et al. (2018) also made sensitivity analyses on the CFD model results by using four different turbulence models. The main outcome achieved from the experimental campaigns performed by Liu et al. (2018) and Albadawi et al. (2018), especially interesting for the objectives of the ELSMOR project, was that

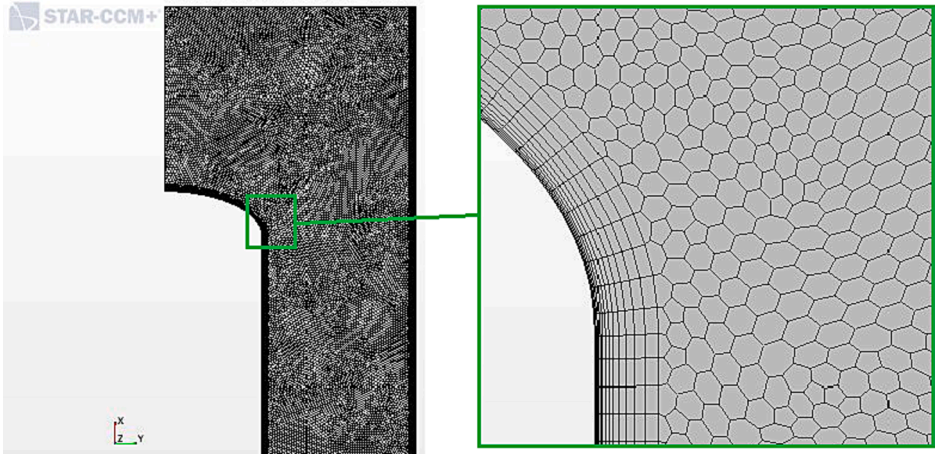

Fig. 3. Adopted 2D mesh in this work for the simulation of Liu et al. (2018) experimental data.

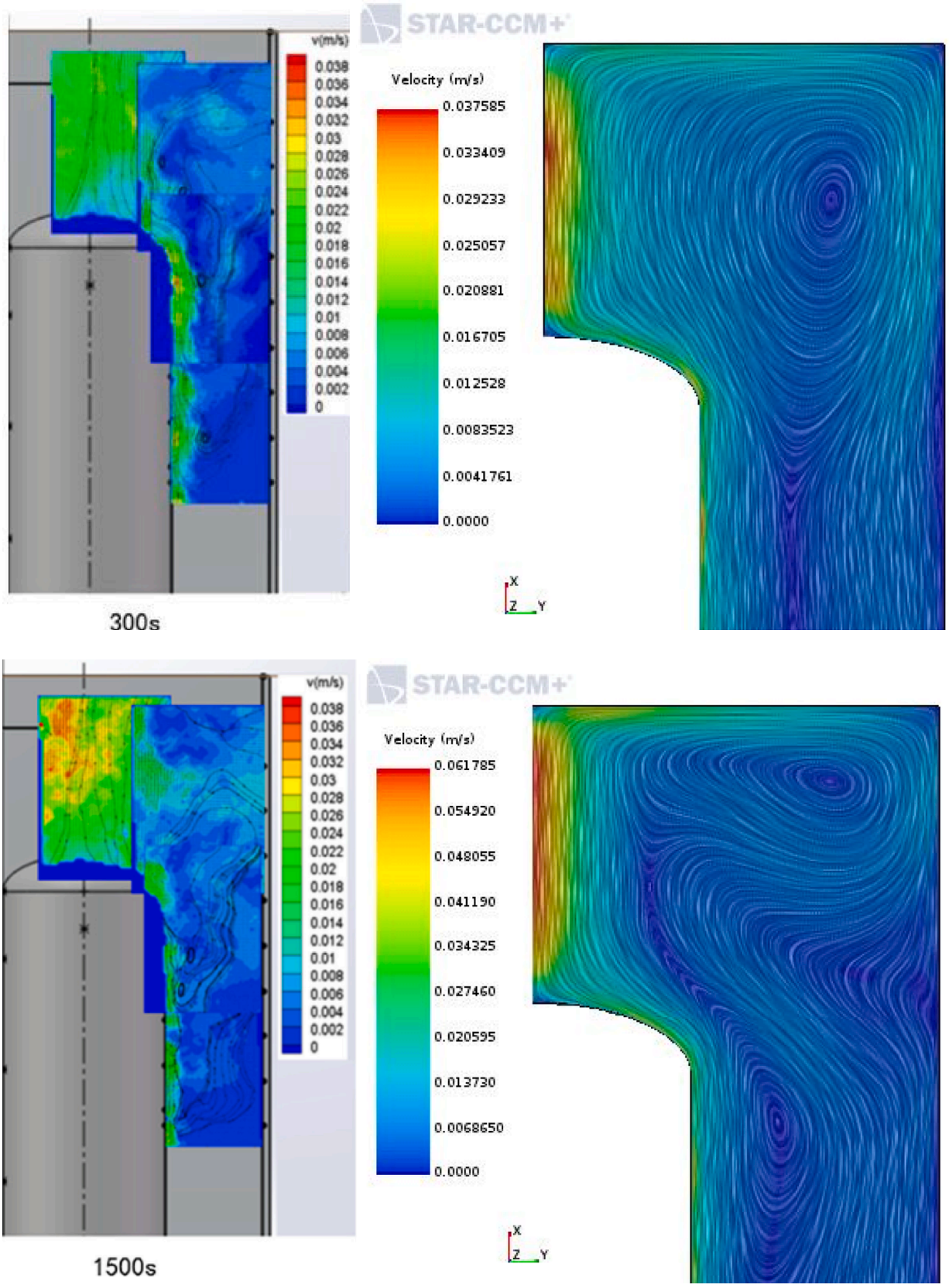

Fig. 4. Comparison of experimental flow patterns measured during the experimental campaign by Liu et al. (2018) (left) and the results from CFD analysis (right) after 300 s and 1500 s of transient time.

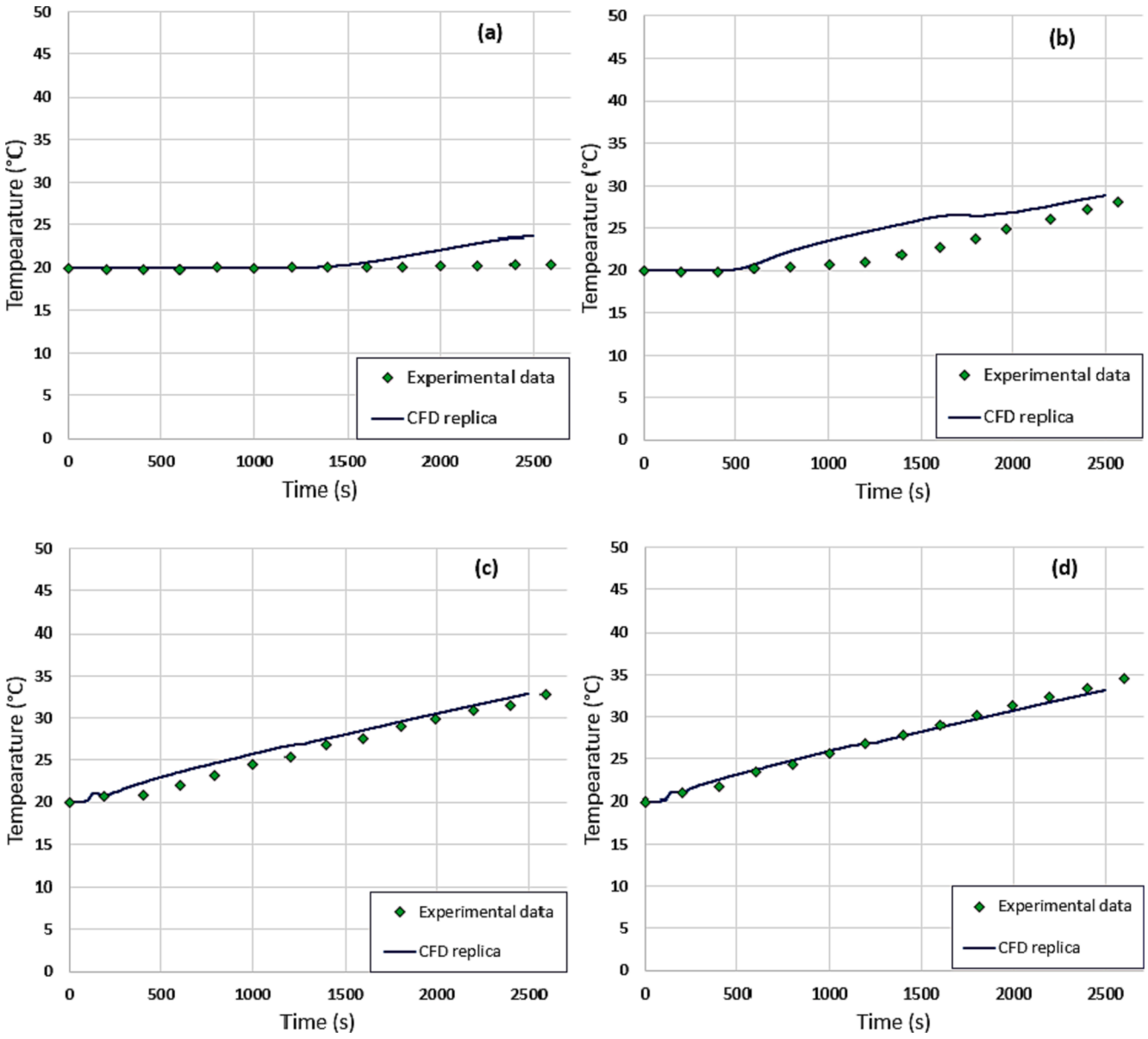

Fig. 5. CFD prediction of water temperature experimental behaviour along the section L2 in Fig. 1 at four different heights: (a) 0.1 m; (b) 0.41 m; (c) 0.87 m; (d) 0.97 m.

a non-negligible thermal stratification inside the pool occurred during the cooling process, while the highest flow velocity was achieved in the plume established on the very top part of the containment. It must be noted that the experiments were run for a maximum of one hour, something that may justify the occurrence of stratification early in such a transient.

Other experimental data collected by a downscaled unit simulating the NuScale Small Modular Reactor (IAEA, 2020) are those described in two MSc theses from Oregon University (OSU) (Casey, 2013; Mullin, 2015), concerning experimental campaigns made on the Multi-Application Small Light Water Reactor (MASLWR) facility (see, e.g., Mascari et al., 2012, for a detailed overview). In these two works, the main focus was on the heat transfer by the inner condensing steam rather than on the water-wall, considering also the influence that non-condensable gases can introduce in terms of an additional resistance to heat transfer. As an example, in the work by Mullin (2015) interesting results were achieved about the influence of non-condensable gases, which were expectedly found to decrease the heat transfer in the bottom part of the containment depending on their initial pressure, due to the path of the outcoming steam that led them to concentrate in the bottom section of the containment.

Besides experimental data focused on the Small Modular Reactor technology as the ones discussed above, others concerning natural convection on vertical surfaces can be found, especially in terms of empirical correlations regarding the main dimensionless parameters involved in the phenomenon (i.e., Nusselt and Rayleigh numbers). For instance, Fujii et al. (1968) collected experimental data in terms of behaviour of the wall temperature and heat flux along a heated wall. In this work, empirical correlations for heat transfer are provided, though the order of magnitude of the Rayleigh number is still far from what is required by the ELSMOR project. In this regard, very interesting results are provided by Kataoka et al. (1992), Kataoka et al. (1994), Kataoka et al. (1995) reporting experimental campaigns on heat transfer established between a suppression chamber and a water wall, which are conceived for use in Light-Water Reactor plants. An interesting aspect of these works is that they assessed a heat transfer correlation for the external natural convection on data obtained with Rayleigh numbers greater than 10^{14} (see, e.g., Kataoka et al., 1992), value which is closer

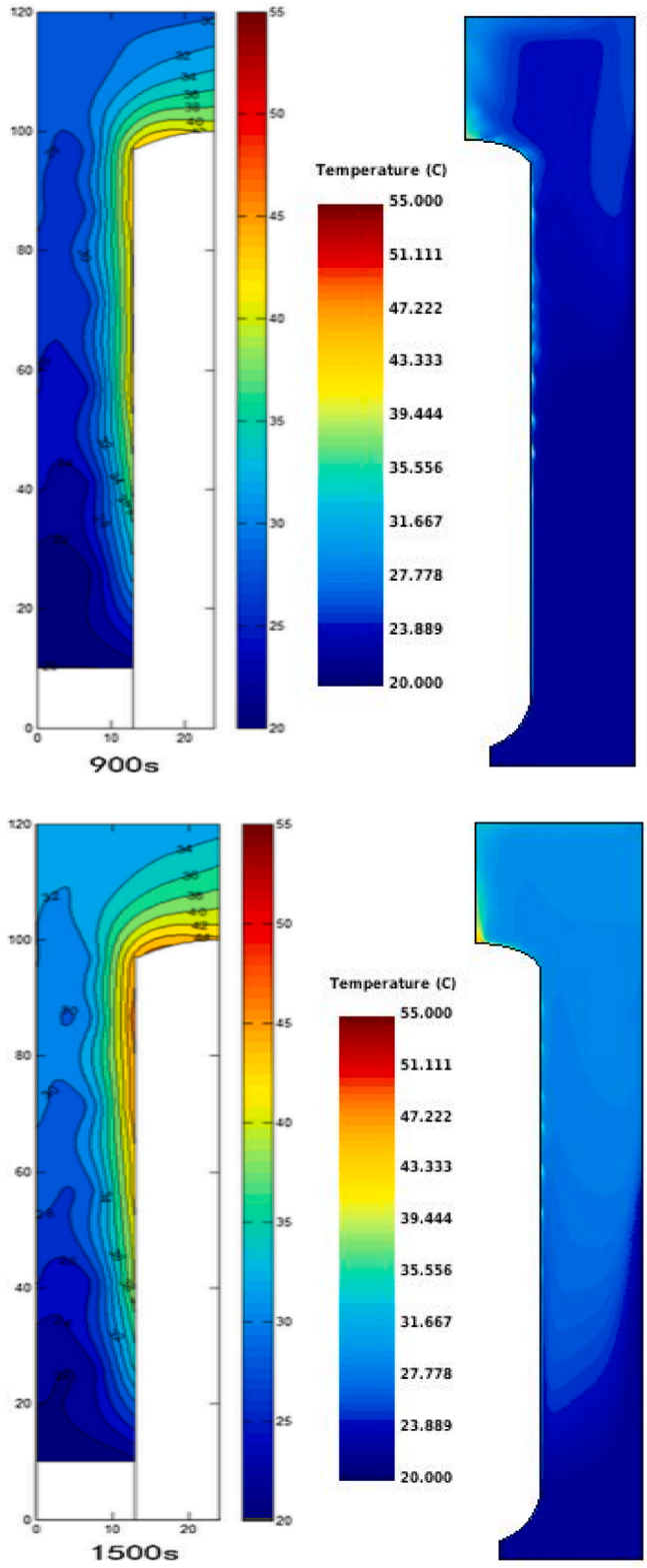

Fig. 6. Comparisons of water temperature field achieved experimentally by Liu et al. (2018) (left) and by the adopted CFD model (right) at two different times: 900 s at the top and 1500 s at the bottom.

to that requested by ELSMOR than the ones of the experimental data discussed so far. The mentioned correlation is the classical "McAdams" one, i.e.:

$$Nu = 0.13Ra^{1/3} \quad (1)$$

According to the authors, the McAdams correlation expressed in Eq. (1) would likely be correct for values of Rayleigh number up to 10^{15}, which is just one order of magnitude lower than the requested one by the subtask 4.2 of the ELSMOR project.

To conclude this brief literature survey, it is clear that available experimental data of interest for the containments of Small Modular Reactors are still scarce. Specific experimental activities have still to be developed to acquire the knowledge necessary to predict the safe behaviour of such passive containments, in view of the interest that the issue is acquiring for the future energy mix. Moreover, even assuming to have achieved enough support for extending the validity of classical correlations to larger values of the Rayleigh number in conventional free convection problems, as may be derived from Kataoka et al. (1992), Kataoka et al. (1994), Kataoka et al. (1995), it is clear that other limitations do exist in the knowledge of the addressed phenomena. For instance, some complexity of the reference geometry and the possible occurrence of thermal stratification inside the pools may pose problems about the efficiency in decay heat removal of containments equipped with passive water-walls, which can be solved only with an adequate experimentation. The interest for better understanding the heat transfer regimes that can be established in the outer containment pools deserves specific experimental efforts, possibly also guided by the numerical exercises which were planned in the frame of the ELSMOR project, to be described below.

3. A first analysis of available experimental data

In order to assess the capabilities of CFD models, the application to some experimental data discussed in Section 2 was carried out. In particular, the experimental data provided by Liu et al. (2018) were considered. As mentioned in the previous section, Liu et al. (2018) performed experimental campaigns on a downscaled unit of the NuScale SMR. In particular, the geometry of both the vessel and the cooling pool was scaled by a factor equal to 1/20, whereas the thermal power was considered smaller by a ratio of 1/8000 obtaining the data presented in Table 1 (from Liu et al. (2018)). Fig. 1 presents sketches of the adopted experimental apparatus together with the location of the most relevant measurement devices.

As it can be noted, the facility consists of a nearly 1 m tall steel vessel with an outer diameter of 219 mm, immersed in a parallelepipedal pool full of water with a square cross section, having a height of 1250 mm and a side of 500 mm. The steel vessel, simulating the containment of the reactor system, is heated by electrical elements along its height, with total powers in the range from 1 to 4 kW. Glass walls are used for the pool and measurements include the use of local K-type thermocouples arranged along specific lines of measurement and of a Particle Image Velocimetry system equipped with a CCD camera, to obtain guesses of the flow patterns in the pool.

Concerning the thermal boundary conditions, Liu et al. (2018) performed experimental campaigns by imposing four values of heating power in the containment (from 1 kW to 4 kW). However, for the application here described only the case with thermal power of 4 kW was addressed in the CFD modelling. At this thermal power, the imposed heat flux at the containment wall was equal to 6231.5 W/m^2 (Liu et al., 2018). For the sake of simplicity, the adopted geometry for the CFD analysis was kept axial-symmetric, as shown in Fig. 1, with an equivalent radius of the pool of 0.2811 m, aiming to preserve the water mass inside the pool.

The boundaries at each surface are reported in Fig. 2; these surfaces were used to impose boundary conditions, coherently with what described by Liu et al. (2018) in relation to their apparatus:

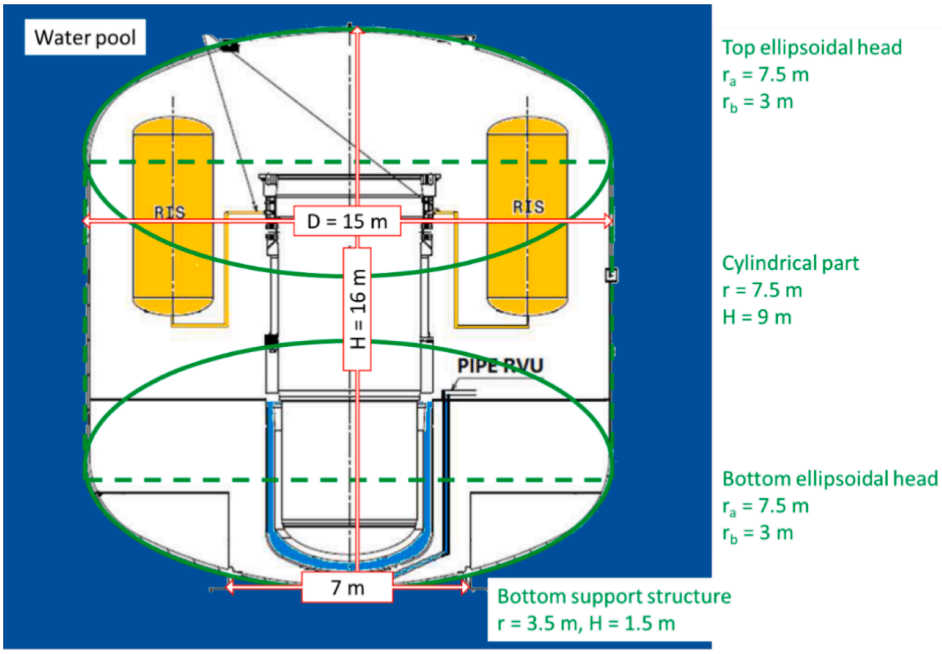

Fig. 7. Geometry of the containment shell proposed in the ELSMOR Academic Exercise.

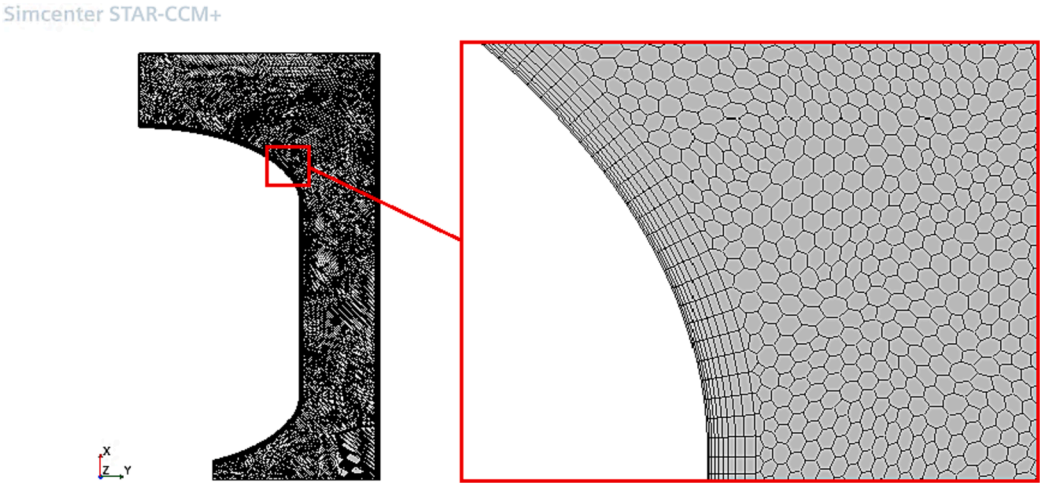

Fig. 8. 2D axisymmetric domain built with STAR-CCM+ and adopted mesh particular.

- on the *Axis* boundary an axial symmetry boundary condition was imposed;
- on the *Containment* boundary, the value of the above specified heat flux was imposed (i.e., 6231.5 W/m^2, corresponding to a total thermal power of 4 kW);
- the *Ground* and *Support* boundaries were considered adiabatic;
- the *Pool Wall* was considered adiabatic as well, as suggested by the authors (Liu et al., 2018);
- on the *Upper Surface* an evaporative heat transfer flux needed to be imposed; concerning its value, Liu et al. (2018) assumed 234 W/m^2; however, in the adopted CFD model the evaporative heat transfer was evaluated by applying a model based on heat and mass transfer analogy (see, e.g., Lienhard, 2020; Incropera and DeWitt, 1996), assuming an environment temperature equal to 295.15 K as suggested by the authors (Liu, et al., 2018). This is necessary because at the surface of the pool one of the most important phenomena to be considered to account for energy losses is evaporation, not directly considered by the CFD code.

The adopted CFD code was STAR-CCM + 16.06 (Simcenter, 2018). Fig. 3 reports the adopted discretisation showing the polyhedral mesh that was used, together with the adoption of prism layers used for refining the nodes close to the containment and pool wall surfaces. The water properties were implemented on the basis of the actual trends (NIST, 2018), avoiding the use of the Boussinesq fluid approximation. The main parameters of the adopted mesh are: a base size of 3 mm, a prism layer thickness of 7 mm, 12 prism layers close to the walls with a stretching factor of 1.25.

A transient analysis was performed by using a time step of 0.005 s with 50 inner iterations. The adopted turbulence model was a Standard $k-\varepsilon$ model with an all-y^+ wall treatment, i.e., a blending of wall functions and a low-Reynolds number approach automatically selected by the code. The choice of the turbulence model was made in order to compromise between accuracy of the results and simplicity of description. The latter was mainly accomplished with by making use of an all y+ treatment, to avoid the need of a considerable mesh refinement close to the wall (impractical for the large size containments), while the

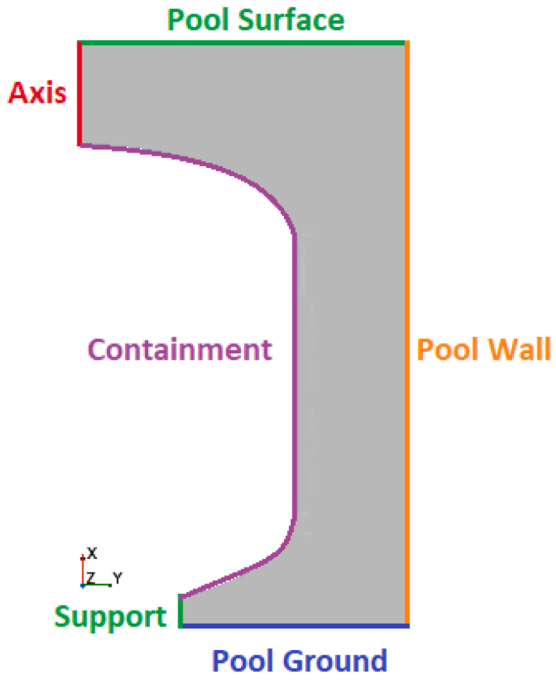

Fig. 9. Boundary surfaces of the 2D domain.

standard k-ε model is just one of the most suggested choices in the STAR-CCM+ code. There was no attempt to make comparisons with different turbulence models, something that could be done in future work to discuss further aspects.

Fig. 4 compares the flow patterns obtained by the CFD analysis with the experimental contour plots provided by Liu et al. (2018) at two different times (i.e., 300 s and 1500 s) in the transient.

As it can be seen from Fig. 4, the overall behaviour of the flow field was reproduced in reasonable similarity, also from a quantitative point of view; this assertion must be considered in view of the uncertainties and of the characteristics of the measuring technique, which provides instantaneous values, while RANS analyses provide time averaged ones.

Another comparison was made for the temperature behaviour achieved along a vertical section of the pool during time (i.e., the section L2 shown in Fig. 1). In particular, fluid temperature was measured at 4 different heights (i.e., 0.1 m, 0.41 m, 0.87 m and 0.97 m) (Liu et al., 2018). Fig. 5 shows the comparison with predictions up to 2500 s.

As it can be noted in Fig. 5, the CFD model was capable of predicting the experimental behaviour of the water temperature with a reasonable accuracy, though in the lower region of the domain the temperature was found slightly overestimated (see the cases at x = 0.1 m and 0.41 m). The overestimation may be related to a possible overprediction of the mixing velocity. As it can be noted from Fig. 4, indeed, besides a moderate overestimation of the plume velocity, the velocity of the water in the entire domain is a bit overestimated by the model (see the velocity scales in experiment and predictions) and this may have led to achieve a greater mixing in the bottom region of the pool.

Finally, to provide a better overview of the temperature predictions, Fig. 6 shows the comparisons between the temperature field of the water wall achieved experimentally and the contours of the same parameter evaluated by the CFD analysis. Despite the involved uncertainties, the reported results show a reasonable accuracy of the CFD model in front of the experimental data, providing confidence in the use of the CFD modelling strategy for the following parametric studies.

4. Scaling up phenomena to a reference design

In the frame of the subtask WP4.3 of the ELSMOR project, an Academic Exercise was proposed with the aim of assessing numerical codes which will be used for simulating the thermal and flow behaviour of the water wall during the passive cooling process. In this frame, an exchange of information between the participants allowed to define the geometrical parameters as well as the boundary conditions to be adopted during calculations aimed at reproducing the phenomena occurring in a full-scale water-wall containment. Fig. 7 shows a sketch of the adopted geometry together with the main dimensions of the addressed system. Though not shown in Fig. 7, the containment is considered to be submerged into a parallelepipedal pool having a square basis with a side of 20 m, full up to a 20 m height with water and bounded all around by 1 m thick concrete walls. The upper atmosphere must be considered full of air and steam, because of evaporation from the pool.

The Academic Exercise was divided into two phases: the first one aims at assessing thermal hydraulic codes without implementing a two-phase flow model, whereas the second part will have as a final objective to consider boiling phenomena. The work presented in this paper refers to the first phase only of the exercise. In coping with the problem, the CFD model considered a single-phase fluid and the simulations were stopped when the saturation temperature was achieved somewhere within the computational domain. Owing to the limited reliability of two-phase models for CFD, the idea to progress the calculation beyond boiling was not considered. For the purposes of the exercise, the saturation temperature was considered equal to 100 °C (i.e., considering 1 bar as reference pressure).

At first, fast 2D analyses were performed by using an axial-symmetric domain, i.e., with a cylindrical pool obtained preserving the water mass; the assumption was obviously that the general behaviour of the water wall should not change too much in an axial symmetry condition with respect to the actual 3D case. Analyses were also made by using a simple model through the system code CATHARE-3 V2.1 (Equipe CATHARE, 2019) in support to CFD calculations, making use of a lumped parameter approach to assess the order of magnitude of different parameters. Finally, 3D calculations were also run, in order to ascertain whether the simplifying assumptions made during the 2D analyses could be considered realistic in view of the actual geometry.

4.1. 2D analyses

The use of an axisymmetric domain relies on the fact that the containment shell has a rotational symmetry with respect to the vertical axis. The 2D analyses served mainly to test the adequacy of the assumed boundary conditions and to guess the timing of occurrence of boiling in the pool, while keeping the computational effort limited. In particular, the pool was considered cylindrical with a circular basis and a height equal to the actual one; hence, the inner radius of the pool was adjusted in order to preserve the mass of water.

The mesh used to perform the 2D analysis by STAR-CCM + 16.06 (Simcenter, 2018) is also in this case a polyhedral one, adopted using prism layers in order to refine the meshes close to the containment wall. The base size of the mesh was set to 8.0 cm (i.e., 250 cells over the pool height and roughly 141 over the pool radius), which resulted an acceptable compromise between accuracy and reasonable duration of each calculation. The prism layer (i.e., the region of mesh refinement close to the wall) was chosen to be 0.2 m thick and contains 9 layers with a stretching factor of 1.25. Fig. 8 represents the adopted CFD domain as well as some features of the generated mesh.

Referring to Fig. 9, where all the domain boundaries are identified, the following boundary conditions were adopted: the *Support* and *Pool Ground* walls were considered adiabatic; the *Containment* wall was considered as a "convection" boundary condition, so that the environment temperature and the heat transfer coefficient can be imposed, including the static thermal resistance of the concrete wall; at the

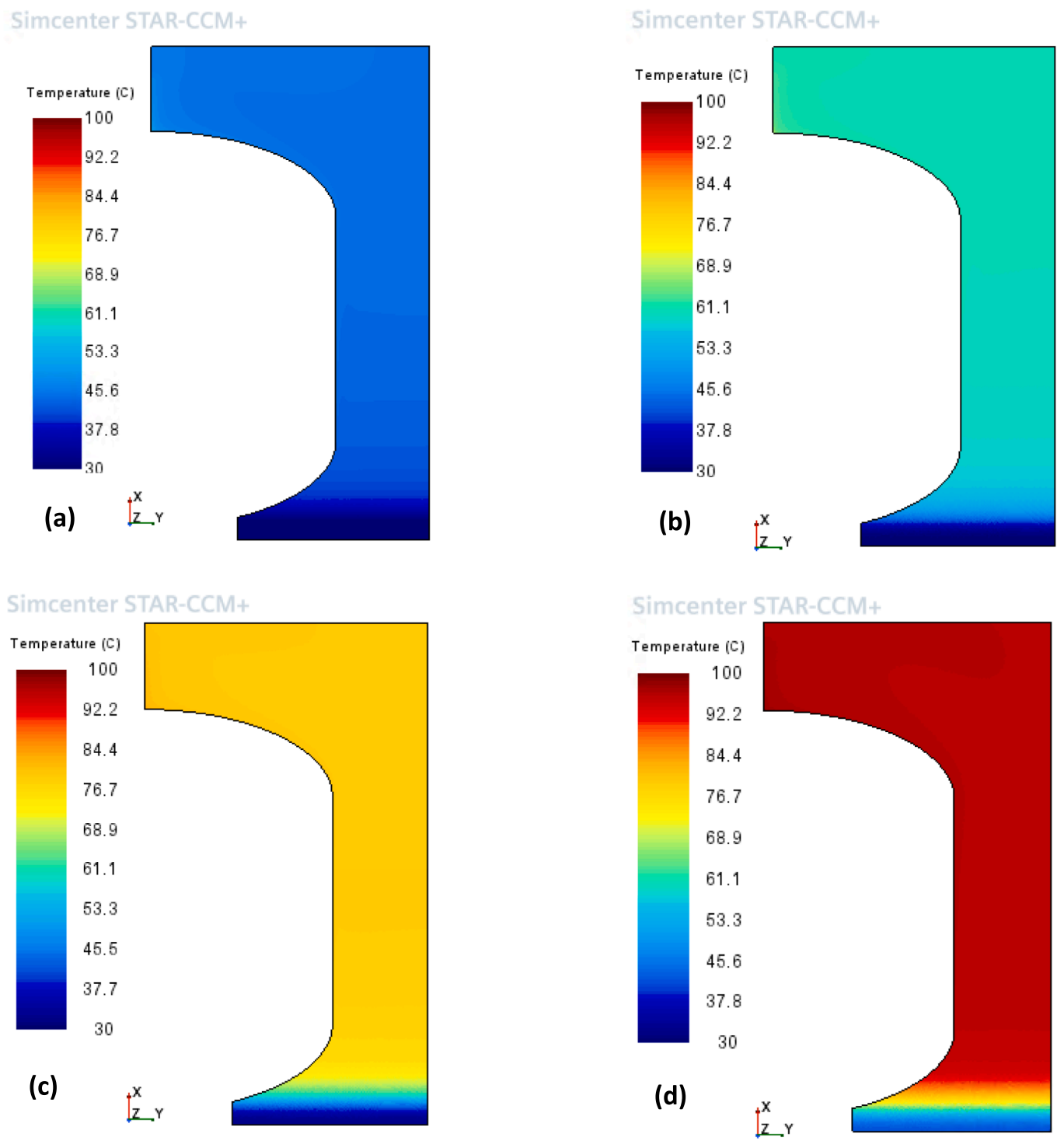

Fig. 10. Temperature fields of the water wall at four different times: (a) 4.5 h, (b) 10.5 h, (c) 19.5 h, and (d) 33 h.

Containment wall an imposed inner temperature (i.e., 133 °C) was assumed. The heat conduction was simulated by an equivalent convection coefficient obtained by considering the thickness of the containment wall (i.e., 0.05 m) and the thermal conductivity of the type 316L stainless steel composing the containment shell. The *Pool Wall* was formally treated as the *Containment* wall, imposing an equivalent thermal resistance based on the concrete thickness and thermal conductivity together with an external temperature (i.e., the temperature of the ground surrounding the concrete walls) assumed equal to 30 °C. Finally, the *Pool Surface* boundary represents the free surface of the pool, at which evaporation takes place, and it was simulated again with a convection boundary condition and a slip boundary wall, i.e., non-zero tangential velocity at the wall. In particular, to evaluate the evaporation losses, the heat and mass transfer analogy was applied (see, e.g., Lienhard, 2020), considering reference conditions in the humid air above the pool and applying a suitable correlation for free convection from a horizontal surface facing an above environment. In order to make the evaporation dependent on the pool surface temperature only, an equivalent heat transfer coefficient was devised, which was imposed for the convection boundary condition set on the pool free surface.

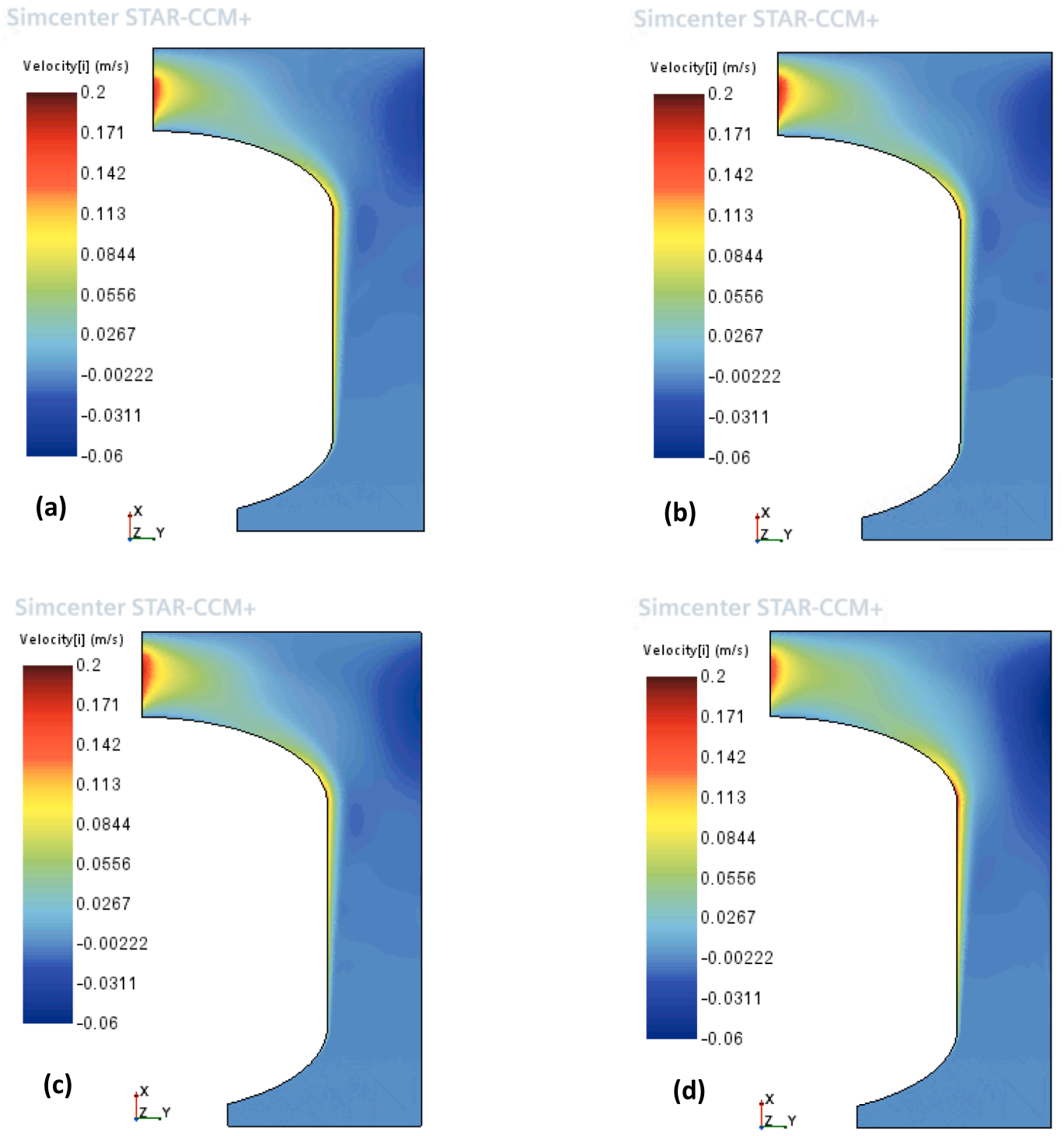

Fig. 11. Vertical velocity field of the water wall at four different times: (a) 4.5 h, (b) 10.5 h, (c) 19.5 h, and (d) 33 h.

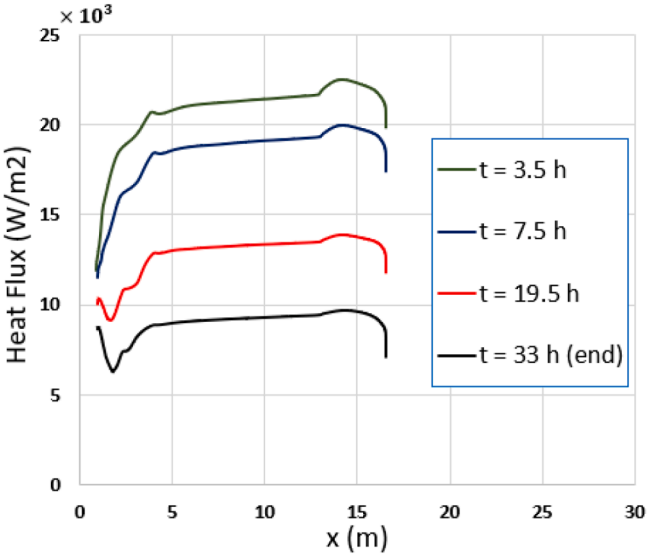

Fig. 12. Heat flux exchanged by the containment with the water-wall at four different times in the transient.

The 2D CFD model thus created makes use of a RANS Standard $k-\varepsilon$ turbulence model with an all-y + wall treatment. Also in this case, in order to make the model better reliable, it was chosen to avoid using the Boussinesq fluid approximation, implementing the actual changes in water properties as a function of temperature by polynomial fittings of their discrete temperature behaviour obtained by the NIST database (NIST, 2018).

First, a steady-state analysis was performed in order to check if any steady condition could be actually achieved with the imposed boundary conditions. Since the behaviour of the water-wall after the start of bulk boiling cannot be analysed with the adopted models, the simulation was stopped when the water temperature reached the saturation value of 100 °C in a certain region of the domain. As expected, no steady state could be achieved since the heat sinks cannot compensate for the large heat source, assumed to be present owing to the boundary conditions imposed to the containment wall.

Following the same rationale adopted during the steady-state analyses, transient analyses were then performed stopping the calculations when the temperature reached saturation somewhere in the computational domain. In the calculations, a time-step of 0.5 s was chosen, using 50 inner iterations. This choice was made with the aim of achieving a reasonable computational time and a sufficiently low value of the residuals at the same time. However, the time-step needed to be lowered after a certain time in the transient (at almost 100,000 s), since the residuals had an unexpected increase, probably due to the changes in fluid properties close to saturation.

In order to understand the thermal behaviour of the water pool, Fig. 10 shows the temperature fields predicted at four different times during the simulation, i.e., at 4.5 h, 10.5 h, 19.5 h and 33 h, where the last time corresponds to the end of the calculation because of detection of the saturation temperature. For the sake of clarity, the temperature scaling is different in every figure.

As it can be seen from Fig. 10, though thermal stratification is observed to occur in the very bottom part of the domain, globally speaking the temperature field was found uniform in a large part of the domain. This can be explained by considering that the heat-up process is relatively long and slow with respect to the previously considered small scale experiment; fluid motion, also favoured by the presence of the lateral concrete wall with its heat losses, seems to generate sufficiently well mixed conditions. The latter result appears to conflict with what was achieved experimentally by Liu et al. (2018) and Albadawi et al. (2018), showing a non-negligible thermal stratification inside the pool. However, it must be mentioned that the experiments carried out by these authors and described in the mentioned works assessed only one hour of the transient, something that could be at the basis of such discrepancies. Indeed, as it was found also in the analyses here described, a time span of one hour might be too small to appreciate the mixing conditions established inside the pool as the time constant of the phenomena is relatively large. Moreover, as it can be seen from Fig. 10, at the end of the simulation most of the water mass was found to be close to the saturation temperature. However, the temperature of some portions of the containment shell resulted to be higher than the saturation value, allowing to conclude that nucleate boiling could reasonably occur even before, depending on the local required superheating.

Concerning the fluid motion, Fig. 11 reports the vertical velocity component field predicted at four different times identical to Fig. 10. As

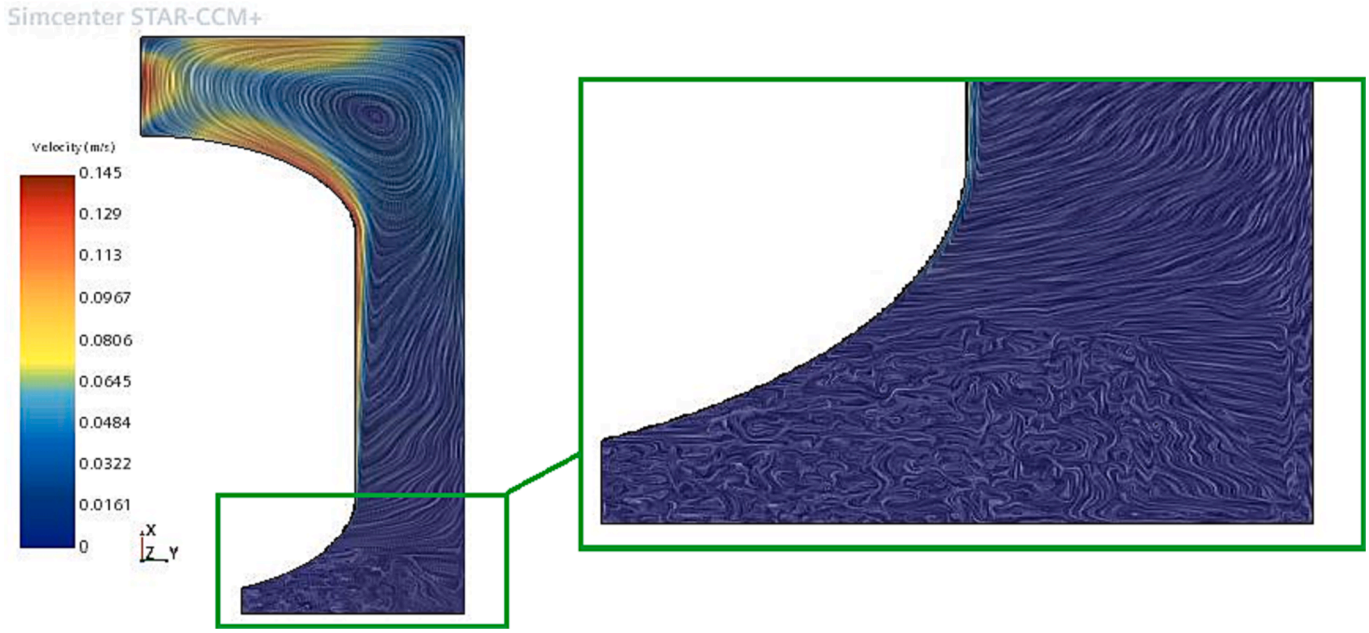

Fig. 13. Streamlines at t = 33 h (end).

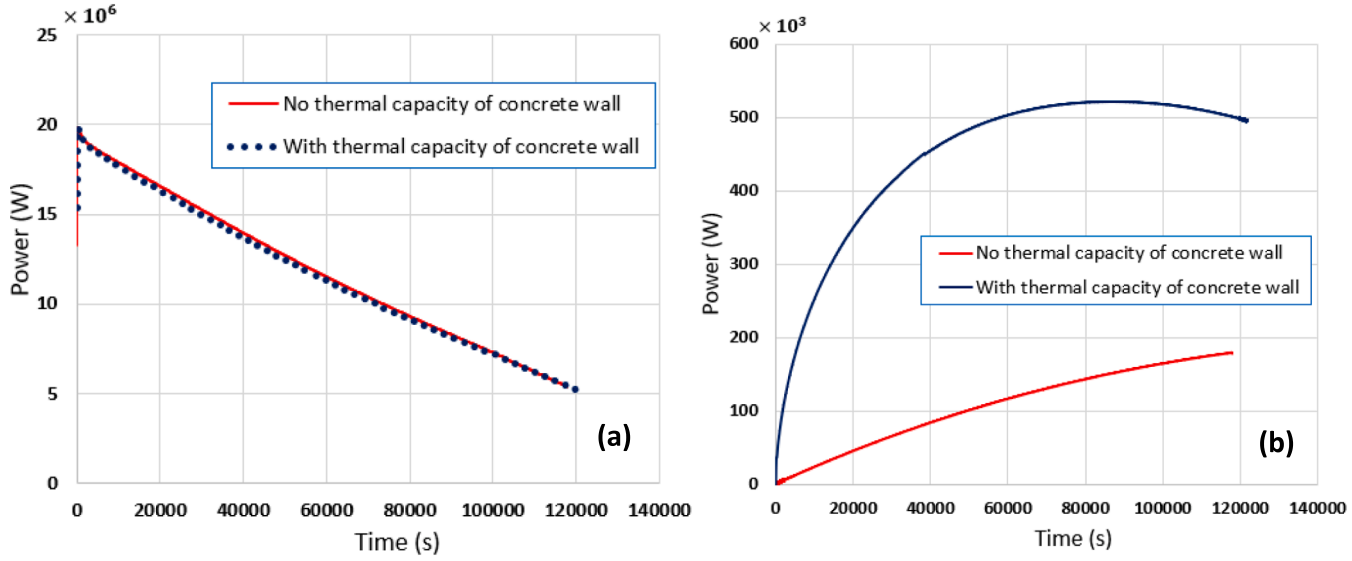

Fig. 14. Comparison of results with and without the thermal capacity of the concrete wall for CFD analyses: (a) net power balance; (b) thermal power losses through the concrete wall.

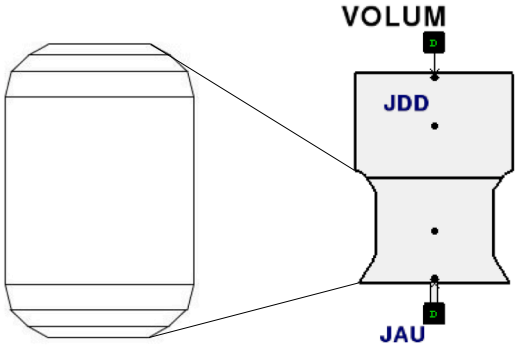

Fig. 15. Sketch of the containment shape adopted in the CATHARE-3 model (left) and 0D domain visualized with the CATHARE graphic interface (right).

it can be seen from Fig. 11, the adopted geometry leads to boundary layer detachment in the region between the end of the containment vertical cylinder and the beginning of the upper dome. The detachment of the boundary layer causes a slight heat transfer enhancement in that region, as it can be seen from Fig. 12, in which the heat flux exchanged by the containment surface is reported.

To complete the panorama of the obtained results, Fig. 13 shows the streamlines at t = 33 h (i.e., the end of the simulation). As it can be seen from Fig. 13, the natural convective motions in the bottom region of the pool become milder with increasing time due to the thermal stratification established in that region, thus leading to a decrease of the heat transfer along the lower dome of the containment, while a convection vortex in the upper part is clearly visible.

In order to check for the effect of the thermal capacity of the concrete wall on the transient behaviour, the model was then equipped with a 1 m thick concrete wall, included in the model by a conjugate heat transfer approach. The adopted mesh for the concrete wall was coherent with the one set up for the pool shown in Fig. 8, i.e., all the mesh parameters were kept unchanged, leading to matching control volumes.

Fig. 14 shows the behaviour of the net power balance obtained by adding all the positive and negative contributions to the energy budget of the system in the CFD model for the addressed two cases, i.e., including and neglecting the heat capacity of the wall. Notwithstanding the difference in the simulated behaviour of the power to the heat structure in the two cases, shown in Fig. 14 (right), it can be noted that the effect on the overall balance is minimal, justifying the neglect of the wall heat capacity in calculations.

4.2. *Lumped parameter analysis with CATHARE-3*

After the 2D CFD analysis, simplified transient calculations were performed by using the system code CATHARE-3 V2.1 (Equipe CATHARE, 2019) aiming at comparing a simpler description of the system behaviour with the results from the CFD calculations. The simplified model was set up using a 0D capacitance volume, i.e., a lumped parameter model available in the code. Since CATHARE-3 does not allow to have ellipsoidal shapes for the heating structures when a 0D model is adopted, the upper and lower domes of the containment shell were approximated by a sequence of truncated cones. On the other hand, the pool geometry was modelled as a square based prism with a side length of 20 m. Fig. 15 shows a sketch of the submerged shell adopted in the CATHARE-3 model as well as the 0D domain visualized by means of the graphic interface of the CATHARE code (i.e., GUITHARE).

The height of the pool volume was actually set equal to 30 m in order to also simulate the humid air environment above the pool itself. The stainless-steel shell of the containment wall was placed in contact with the lower sub-volume of the considered hydraulic component. Starting with a steady state with the pool volume full of liquid, during the transient analysis the domain was firstly emptied to bring the mixture level to 20 m, thus simulating the cooling pool as well as the upper environment. In order to simulate the ambient air above the pool, non-condensable gas was considered to be present in the upper volume. The boundary conditions of the lumped parameter model were defined in similarity with those used during the CFD analyses described in the previous sections, with the only difference of having considered the pool walls adiabatic and with the evaporation model at the free surface, specified by CATHARE own models.

Fig. 16 reports the comparison of the temperature calculated for the lower subvolume of the lumped parameter model of CATHARE (i.e., the part of the model that simulates the water-wall) with the mass averaged water pool temperature obtained by the 2D CFD model. As it can be noted, expectedly the two trends differ, however remaining qualitatively similar. Among the contributors to the observed differences, in addition to the basic diversity of the two models (distributed parameter and

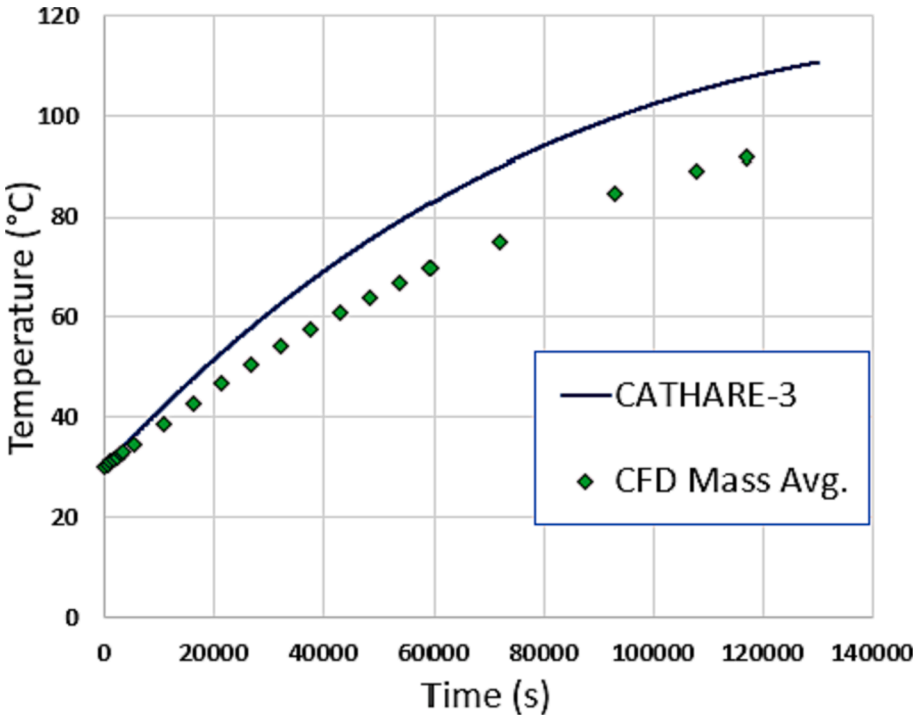

Fig. 16. Comparison between the water temperature obtained from CATHARE-3 and the mass averaged temperature from the CFD calculation.

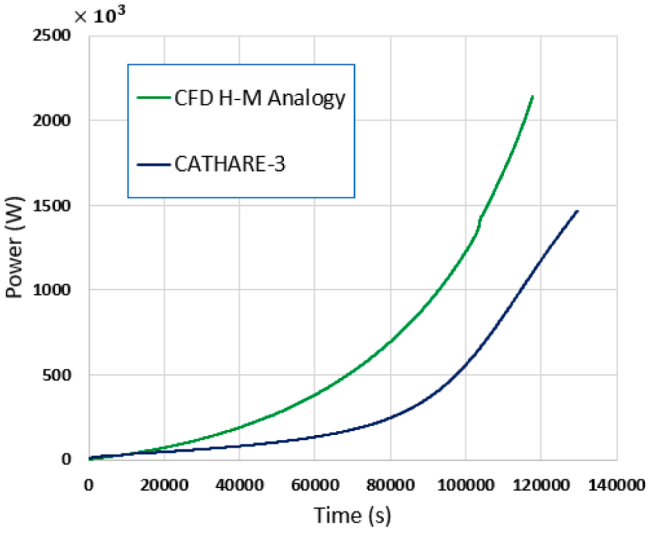

Fig. 17. Evaporative power losses for CFD and CATHARE-3 analyses.

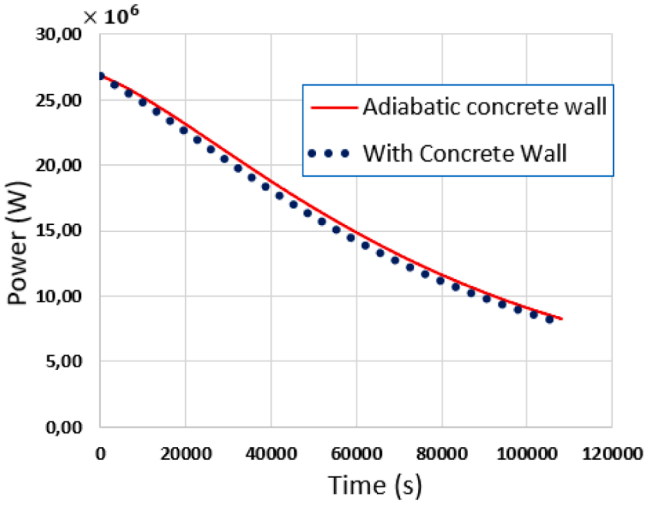

Fig. 18. Comparison between the net power balance behaviour achieved with CATHARE-3 for the two analysed cases.

lumped parameter ones), also the treatment of the evaporation rate at the pool surface is playing a role. In the case of CATHARE-3, the interface is facing an environment which was let to be washed of the initially contained air by the evaporated steam as in an open containment pool (an assumption adopted in the analysis which could be easily changed if needed), giving rise to an atmosphere richer and richer with steam, thus increasing steam partial pressure, that progressively decreased the evaporation rate. The different evaporative heat transfer evaluated by the CFD model and by CATHARE-3 are shown in Fig. 17; indeed, the averaged evaluation of the pool surface temperature for a lumped parameter model and the local one for a CFD model result in different representations of the phenomena, making the comparison only an order of magnitude check of the quantitative values.

In a further analysis, also in the CATHARE-3 model the concrete wall was implemented, adopting the same rationale used for the CFD analyses described above. The adopted external wall was considered planar with a height of 30 m, i.e., it covered the entire height of the volume domain. The properties of concrete adopted in the analysis were assigned making use of the library available in the CATHARE-3 code. The thickness of the structure (i.e., 1 m) was divided into 20 nodes and on the outer side of the slab a convective condition was imposed as the one adopted for the containment structure, imposing a large value of the heat transfer coefficient to result de facto in a Dirichlet boundary condition with an outer wall temperature of 30 °C. All the other boundary conditions were kept unchanged.

The simulation with the concrete wall covered 30 h of real transient time. Fig. 18 shows the comparison between the net power balance behaviour obtained with CATHARE-3 for the two cases. As it can be

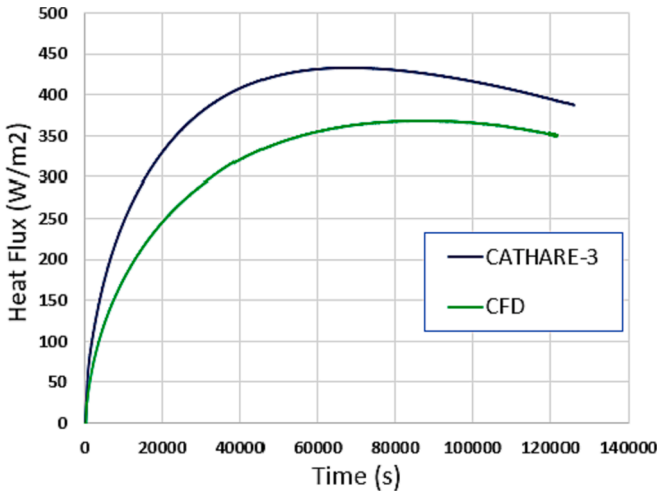

Fig. 19. Heat flux lost through the concrete wall from CFD and CATHARE-3 analyses.

seen, even in this case only slight differences were obtained by considering the presence of the concrete wall, confirming a minor role in the overall behaviour. A comparison of the heat transferred to the concrete wall in the CFD and in the CATHARE-3 calculations is reported in Fig. 19, showing a general coherence in view of the differences of the adopted models.

4.3. 3D CFD analyses

A transient three-dimensional CFD simulation was then performed by using STAR-CCM+ (Simcenter, 2018). The main objective of this further phase of the study was to assess the behaviour of the water-wall by considering a square-based pool instead of a circular and axi-symmetric one, in order to analyse possible 3D phenomena which could not be considered by the 2D simulations. Fig. 20 shows the adopted computational domain together with a detail of the generated mesh.

In order to limit the needed computational resources, only 1/8 of the actual geometry was considered to perform the calculation (see again Fig. 20), taking profit of an evident octant symmetry of the addressed system. A coarser mesh was also tolerated with respect to the one adopted for the 2D analyses, increasing the base size to 16 cm, whereas the type of the mesh was still kept polyhedral, making use of prism layers in order to refine the mesh close to the containment surface.

Boundary conditions were adopted in coherence with the 2D analyses for purpose of close comparison. In this case, the presence of the pool wall was simulated by imposing an equivalent thermal resistance (i.e., by neglecting its thermal capacitance) in order simplify the calculation. The two lateral vertical surfaces, instead, were considered as *symmetry planes*. Concerning the turbulence model, also in the 3D analysis a Standard $k-\varepsilon$ model was used together with an all-y^+ wall treatment for the cells close to the wall. The transient analysis was carried out by considering a time-step of 2.5 s adopted with 50 total iterations, found to be a good compromise between accuracy and duration of the calculations.

Fig. 21 shows the trend of the net power balance of the 3D model compared with that achieved through the 2D analysis showing close coherence. The calculation was stopped after 10.5 h of simulated time of the cooling process and it was carried out by using 12 CPU cores in parallel: the entire analysis lasted nearly 4 days. The choice of simulating only a part of the transient was made, comparing the results of the early phase of the 3D calculation with those of the previous results of the 2D CFD analysis, having as a purpose to check if the global behaviour predicted by the 2D and the 3D models was similar. In particular, the mixing effects pointed out by the 2D analyses were checked, e.g., representing the temperature distributions along two vertical sections placed on the two lateral symmetry planes (see Fig. 22) and located at intermediate distance between the containment steel shell and the concrete wall. Fig. 23 reports the distribution of the water temperature at two different times (i.e., 4.5 h and 10.5 h) along the two lines.

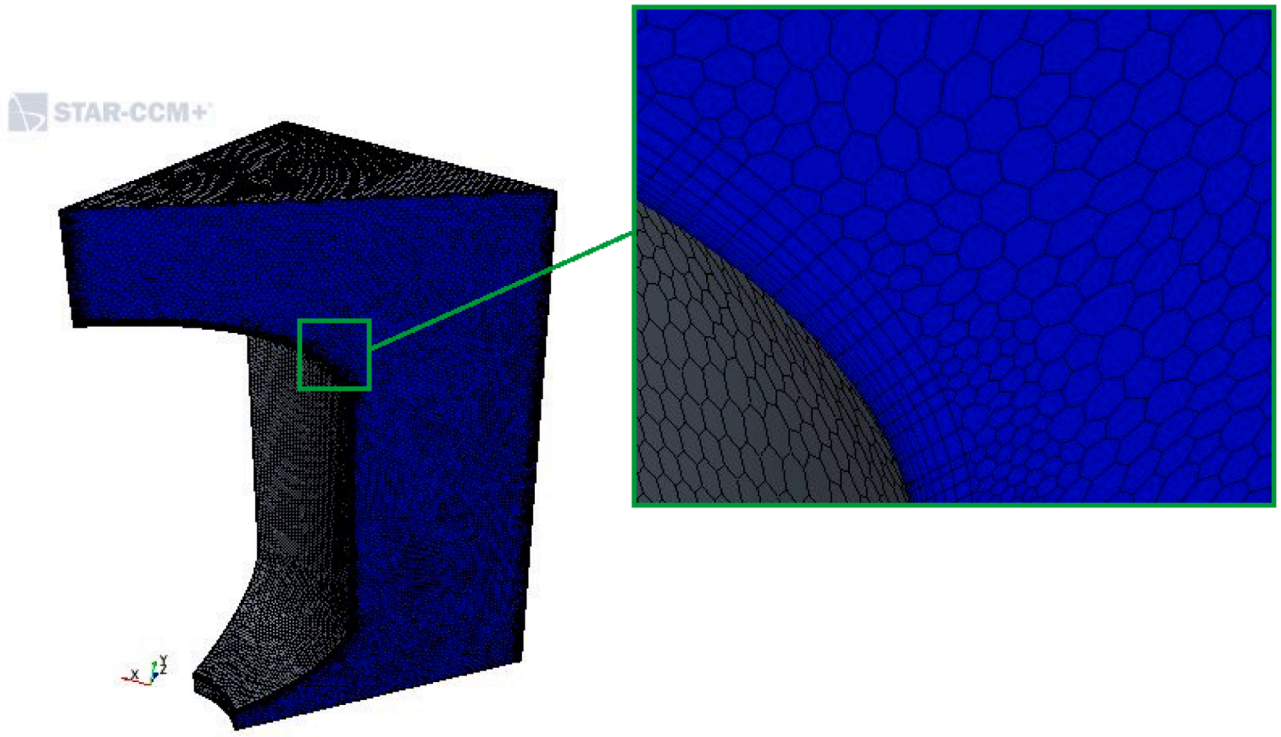

Fig. 20. 3D computational domain and adopted mesh.

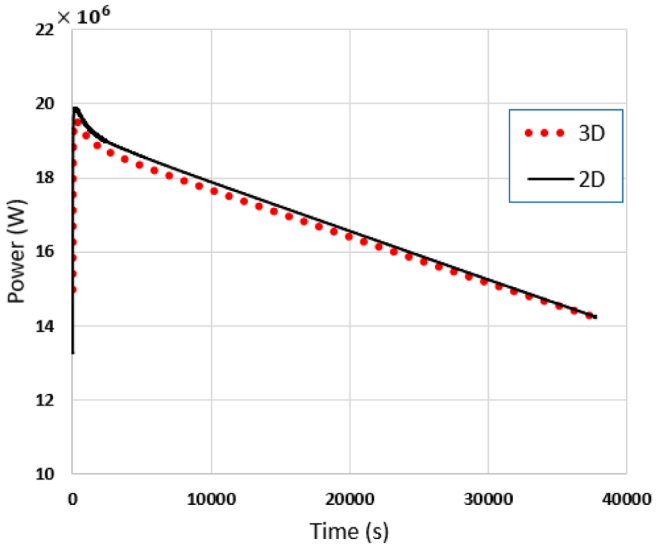

Fig. 21. Comparison between the power balance behaviour for the 3D and 2D cases.

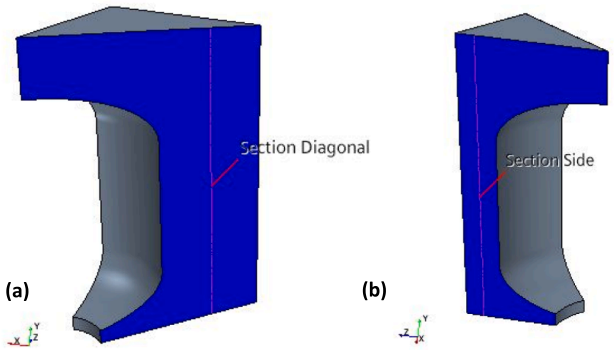

Fig. 22. Vertical sections of the domain: (a) vertical section on the diagonal symmetry plane; (b) vertical section on the side symmetry plane.

As it can be seen from Fig. 23, the thermal stratification achieved in the pool is generally negligible, even though it cannot be neglected in the very bottom part of the domain, a result already noted in the 2D analyses. An interesting difference between the 3D and 2D analysis is that the thermal stratification established in the bottom part of the pool seemed to break during time as shown in Fig. 24, where the comparison between the 3D and 2D temperature behaviour on the pool vertical section is shown. This phenomenon seems to be caused by a 3D effect due to the presence of the heat losses through the concrete wall, which cause an increase of the recirculation velocity in the bottom part of the pool leading to a better mixing of water in that region than in 2D conditions. The angle formed by the two planar walls, indeed, may lead to a higher cooling of water by heat losses in that region, thus causing a greater average downward velocity.

For the sake of completeness, Fig. 25 shows the temperature fields predicted for the two symmetry surfaces of the 3D domain after 4.5 h of reactor time, showing great similarity with what was obtained by the 2D analyses described in the previous sections.

Similarly, Fig. 26 shows the vertical velocity fields at the same time; even for this comparison the similarity between the 3D and 2D simulations is somewhat evident. As it can be seen from Fig. 26, even though the velocity field is slightly different in terms of the highest and lowest values achieved, its global behaviour is quite similar in the two cases. The differences among the lowest values (considering the negative sign) of the velocity can be explained again with the higher mixing established in the bottom part of the pool already noted above for the 3D case.

Finally, Fig. 27 shows the temperature distribution on the upper surface of the pool at the end of the simulation (i.e., 10.5 h) together with the behaviour of the related power losses during the transient. As it can be noted, the estimated powers for the 2D and the 3D cases are quite similar.

In summary, the differences between the predictions obtained by the 2D and 3D models seem to be quite limited, thus justifying the adoption of the former for faster analyses related to the overall behaviour of water wall systems.

5. Scaling considerations

After the analyses shown in the previous sections, additional studies were carried out for downscaled domains aiming at understanding if a homothetical change in the dimensions of the containment wall and of the water-wall complex could give rise to similar phenomena at different scaling. This was obtained by halving and dividing by four times the linear size of the model adopted for running 2D analyses of the full-scale exercise and comparing the obtained results in various forms.

The scaling of the original domain by factors 1:2 and 1:4 was easily achieved by making use of the tools available in the CFD code for

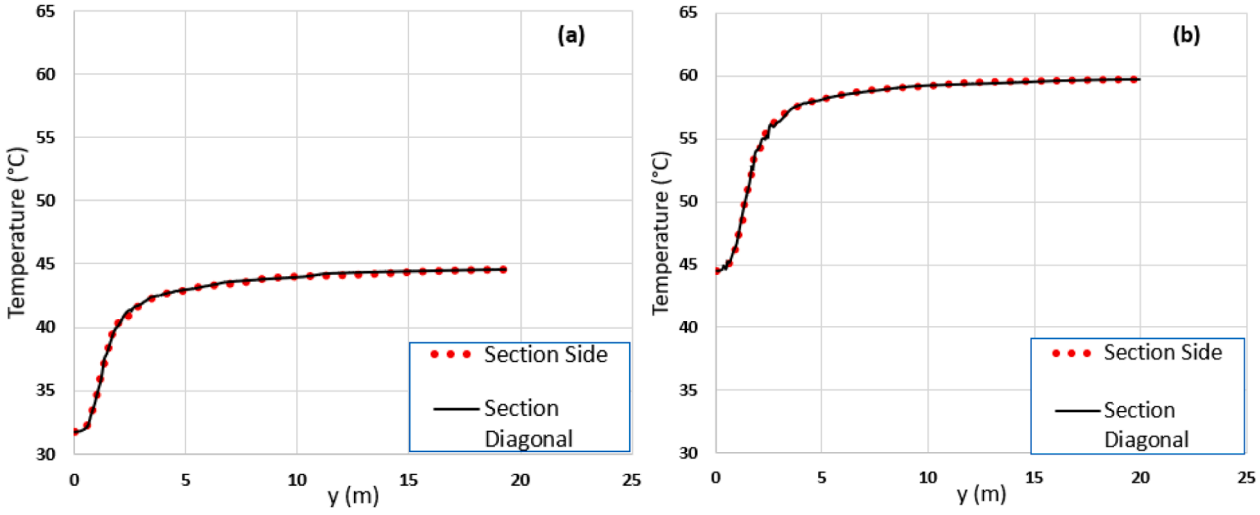

Fig. 23. Temperature distribution along the vertical sections at two different times: (a) after 4.5 h of cooling process; (b) after 10.5 h of cooling process.

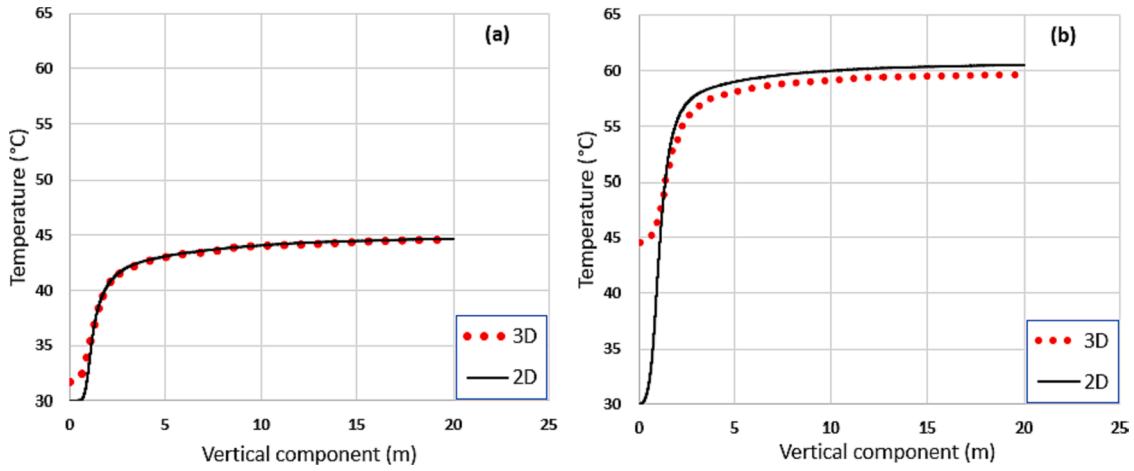

Fig. 24. Comparison between 3D and 2D temperature on a vertical section of the pool at two different times: (a) after 4.5 h of cooling process; (b) after 10.5 h of cooling process.

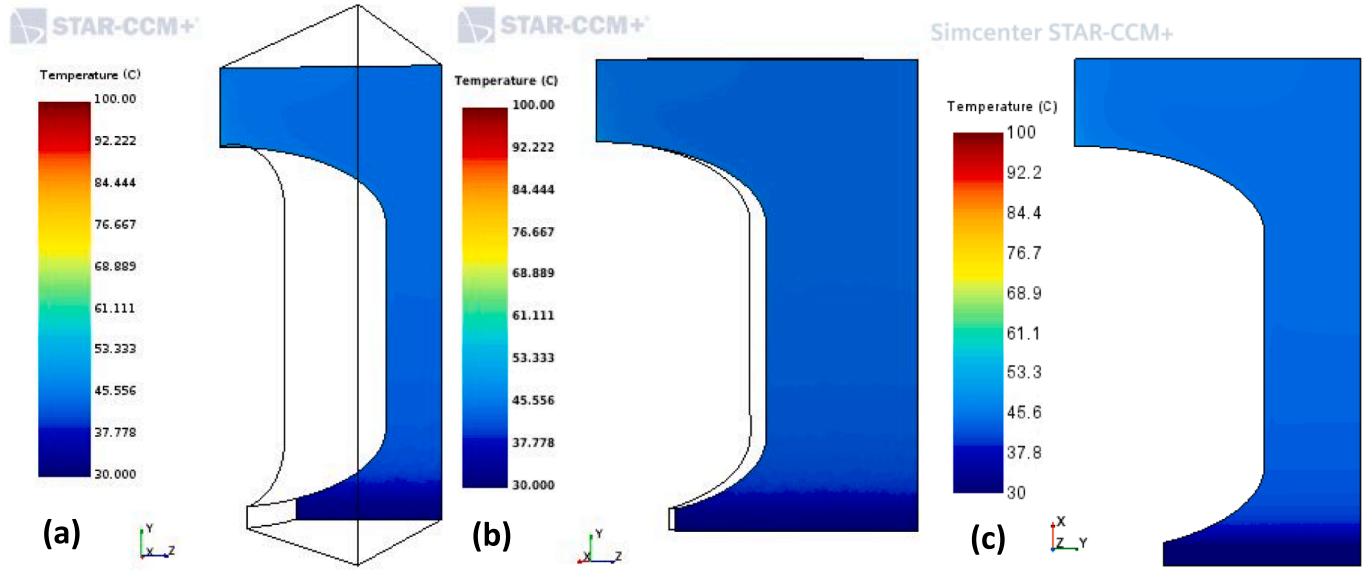

Fig. 25. Comparison between the temperature field in both 3D and 2D analyses for t = 4.5 h. (a) Side symmetry plane; (b) Diagonal symmetry plane; (c) 2D domain.

transforming geometrical domains; together with the domain, the adopted STAR-CCM+ code also scaled the original mesh, keeping some of its parameters unchanged despite of the different size (i.e., number of cells, growth ratio in the prism layers and so on). Therefore, for the downscaled domains the meshes were smaller than in the full-scale case and also the time step used for the transient analysis was decreased. In particular, for the domain with a 1:2 scale the chosen time-step was 0.25 s whereas for the case with a 1:4 scale it was 0.1 s, both simulated through 50 iterations. The choice of the time-steps was again dictated by the rationale of having sufficiently low values of the residuals together with a reasonable duration of each simulation. Fig. 28 illustrates the configurations of the addressed domains together with the adopted mesh.

Downscaling was also applied to some of the boundary conditions involving the containment and the concrete wall thicknesses with "convection" boundary conditions. The boundary condition on the free surface, instead, was kept unchanged as it depends on the water temperature rather than on geometrical quantities: indeed, the surface area is downscaled as a consequence of the mentioned linear scaling.

As in the previous analyses, the simulations were stopped when the saturation temperature of 100 °C was achieved somewhere in the domain. In Table 2, the time requested for the pool to start boiling is reported for each of the addressed cases:

Furthermore, Fig. 29 shows the behaviour of the net power balance vs transient time.

Similarities pointed out by the analyses concern the velocity fields achieved in the downscaled domains. As it can be seen from Fig. 30, despite of expected quantitative differences, the general flow pattern is pretty similar in each case analysed with respect to the full-scale one shown in Fig. 11.

As it can be noted from Fig. 31 and Fig. 32, similarly to what was obtained from the previous analyses for the full-scale domain, the thermal stratification in the pool appears negligible, except at the very bottom where the recirculation of water is damped leading to a decrease of heat transfer.

6. Conclusions

In this work, CFD analyses have been performed with different assumptions, boundary conditions, and length scales in order to explore the behaviour of nuclear reactor containments equipped with water walls, as those proposed for some Small Modular Reactors presently

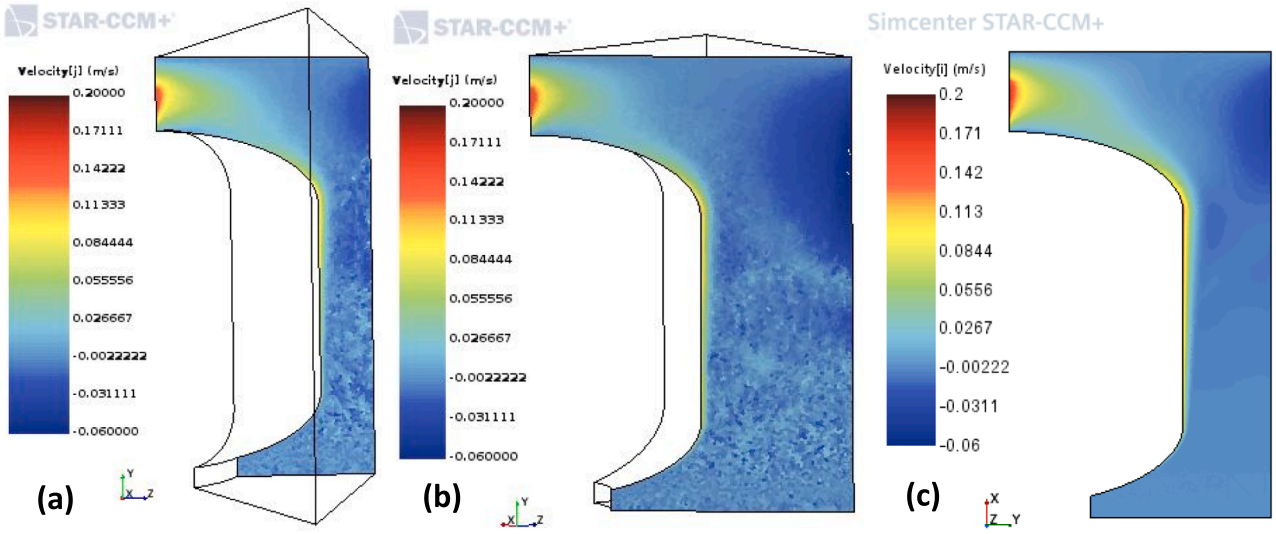

Fig. 26. Comparison between the vertical velocity fields in both 3D and 2D analyses at t = 4.5 h. (a) Side symmetry plane; (b) Diagonal symmetry plane; (c) 2D domain.

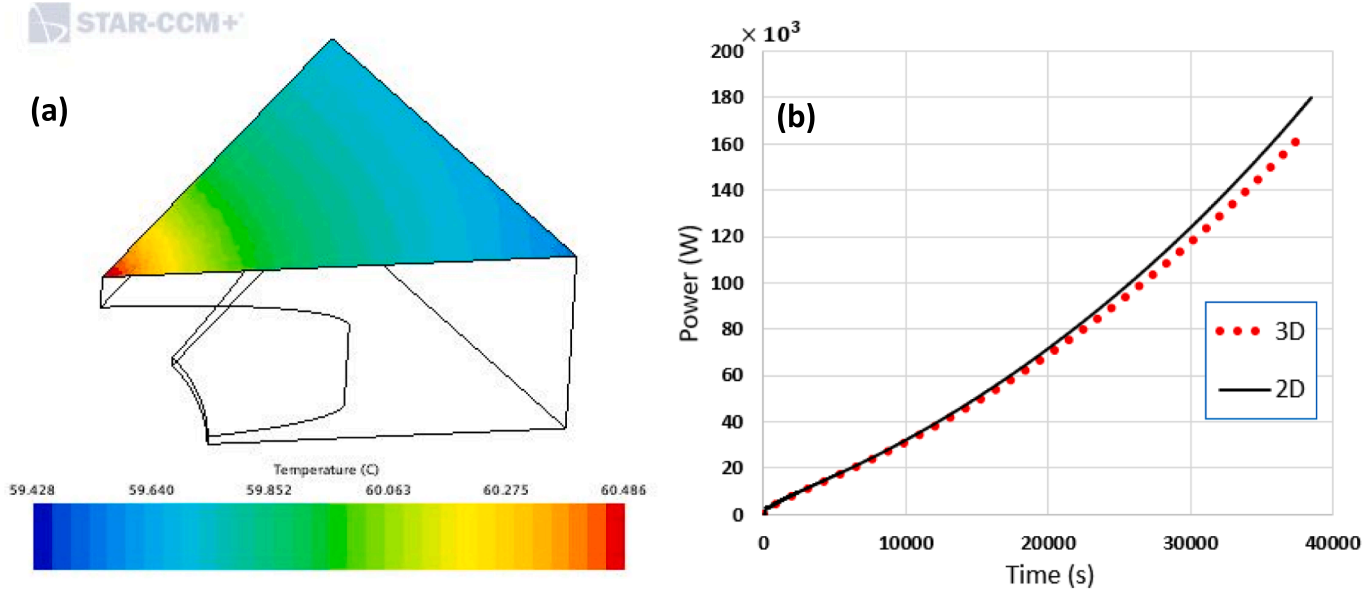

Fig. 27. (a) Temperature field on the pool free surface for t = 10.5 h, and (b) comparison between the related power losses between 2D and 3D analyses.

under development.

The lack of an extended experimental database applicable to these phenomena motivated the study, which started from the scarce available experimental evidence to provide a reasonable degree of validation of the adopted numerical tools. The obtained results were extrapolated making use of the prediction capabilities of numerical models, trying to envisage the unknown range of phenomena for full-scale reactor pools. While the obtained information can be considered incomplete in the lack of applicable experimental data, it nevertheless provides a guidance to deal with phenomena that are presently out of reach in terms of supporting experimental evidence.

The rationale adopted in setting up models for studying the addressed system involved different tools, geometry and assumptions. Two-dimensional and three-dimensional calculations were performed, trying to highlight the differences in their capabilities to reveal key behaviours. A lumped parameter model was also used in support, developed making use of a well-assessed thermal–hydraulic code usually applied in complex NPP accident calculations, in the aim to check that the order of magnitude of global phenomena was not lost in the simulations performed by more detailed CFD codes. Considering that experimental facilities are and will be available only in small scales, a simple scaling analysis was conducted, by homothetically shrinking the full-scale model to smaller sizes. It is necessary to note that, in order to reach full scale size with a CFD technique, large meshes were tolerated, something to be always considered with due care in view of possible truncation error effects and model extrapolation; however, the scaling process performed with smaller sizes and meshes seems to provide confidence that, in view of the usual convergence checks, the predicted phenomena are similar at different scales and mesh sizes, supporting the general correctness of the analysis.

A variety of boundary conditions was also adopted, e.g., in the treatment of the lateral concrete walls, which could not be ignored and which were represented as simple heat transfer resistances or more reliably as bodies possessing both conductivity and volumetric heat capacity. Particular relevance was ascribed to the simulation of the heat losses by evaporation at the upper surface of the water pool, setting up a

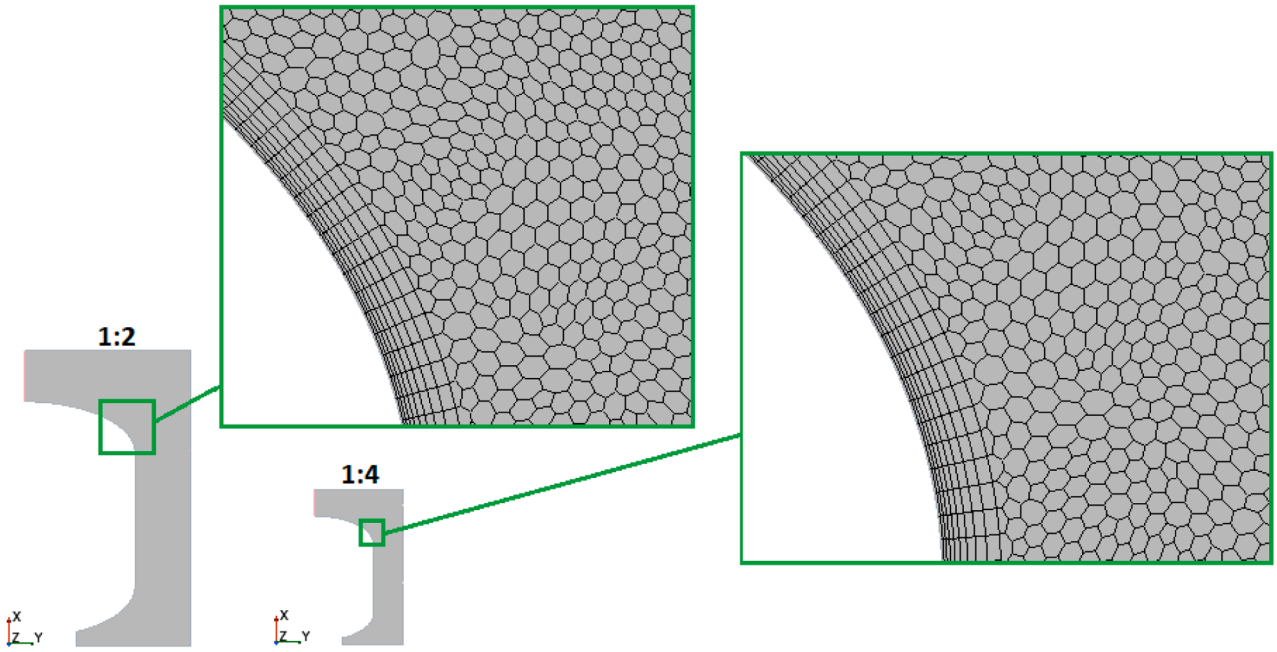

Fig. 28. Downscaled domains and adopted mesh.

Table 2
Time requested by the pool to boil in each scale.

Scale	Time to reach bulk boiling (s)	Time to reach bulk boiling (h)
1:1	118,000	32.7
1:2	26,000	7.2
1:4	9,000	2.5

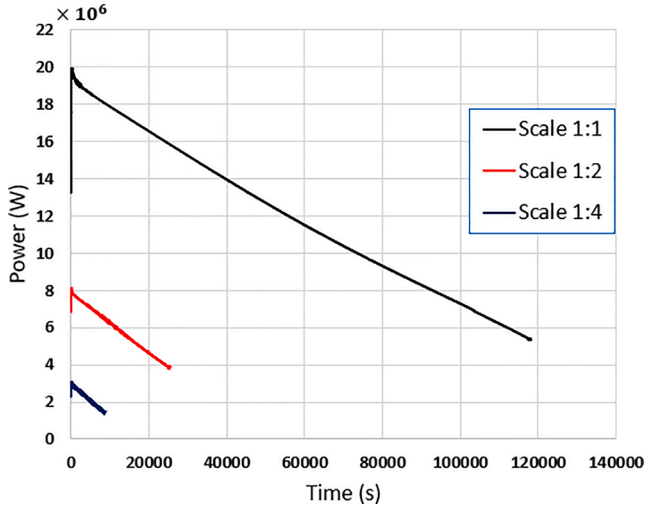

Fig. 29. Net power balance behaviour during time.

detailed model based on the analogy between heat and mass transfer, capable to assign to the upper pool surface the best possible estimation of the energy lost by latent and sensible heat transfer.

The obtained results show, as a relevant feature, a considerable degree of mixing in the containment water pool, as a consequence of the very slow but persisting convective motions that occur along its height, mainly promoted by the natural circulation loops established also owing to the lateral heat losses and to the evaporation at the free surface. This

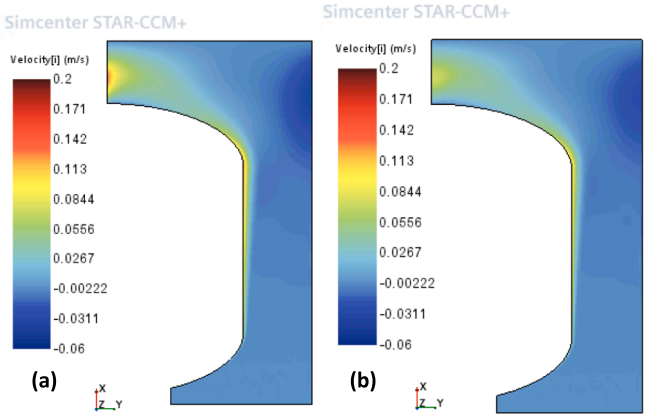

Fig. 30. Vertical velocity field in downscaled domains achieved at the end of each simulation for two different scales: (a) 1:2, and (b) 1:4.

phenomenon, which appears to be particularly favourable in view of safety, owing to the involvement of large masses of the water pool in the decay heat removal processes, suggests an issue worth of further attentive assessment to be confirmed or denied, owing to its relevance in the long-term analyses of station black-out scenarios that SMRs will be particularly targeted to counteract.

In the frame of the ELSMOR project, an outcome of this work and a possible continuation of the same line of research could be the study of the margins for the release of decay heat via the water wall, considering more realistic boundary conditions to be imposed to the inner surface of the containment, in order to evaluate a station blackout scenario: this will provide matter for future work.

CRediT authorship contribution statement

Alessandro De Angelis: Formal analysis, Investigation, Writing – original draft. **Nils Reinke:** Validation, Methodology, Writing – review & editing. **Walter Ambrosini:** Supervision, Methodology, Writing – review & editing.

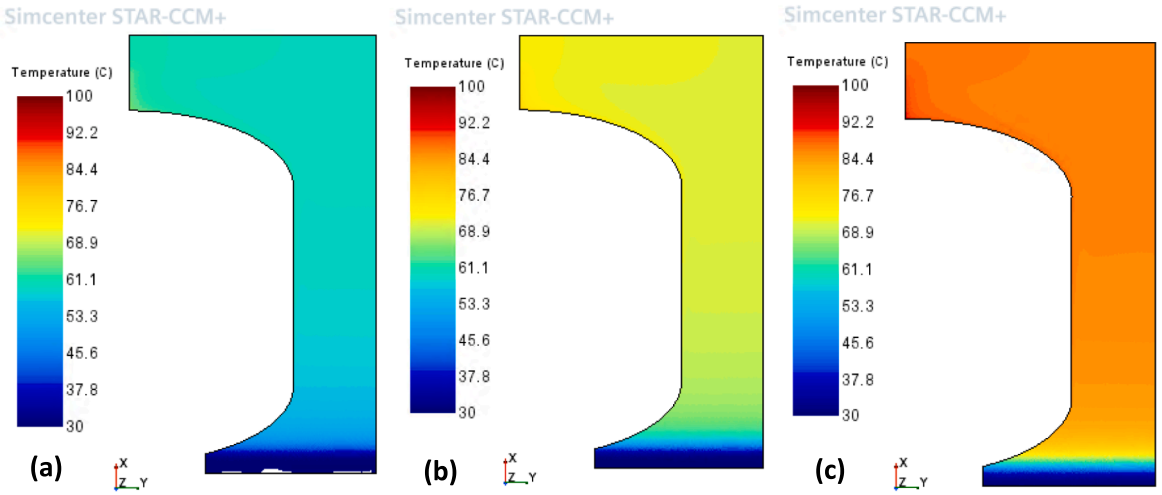

Fig. 31. Temperature field achieved in the downscaled case (1:2) at different times: (a) 10,800 s, (b) 16,200 s, (c) end of simulation.

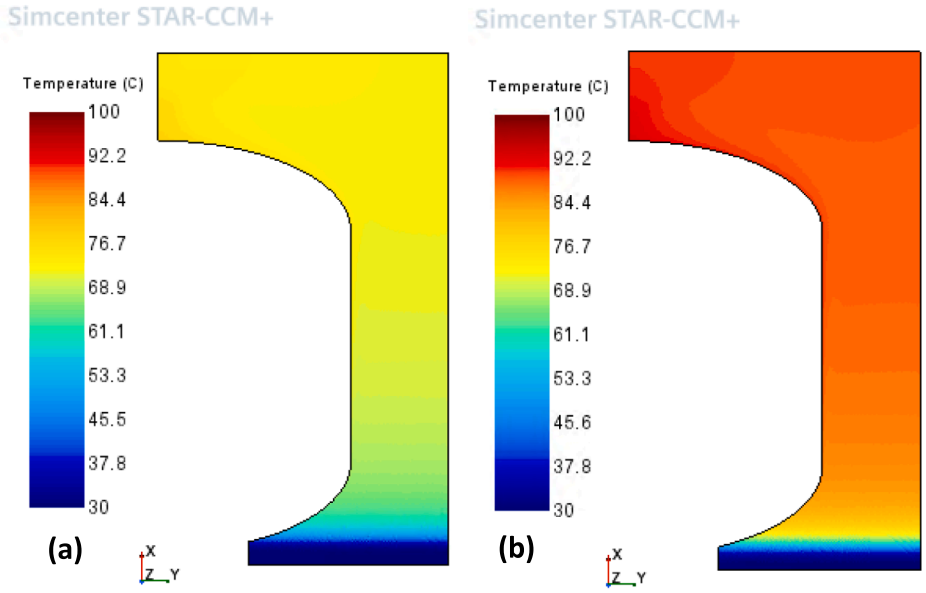

Fig. 32. Temperature field achieved in the downscaled case (1:4) at different times: (a) 5400 s, (b) end of simulation.

Declaration of Competing Interest

The authors declare the following financial interests/personal relationships which may be considered as potential competing interests: Walter Ambrosini reports financial support was provided by European Commission. Alessandro De Angelis reports financial support was provided by Government of Italy Ministry of Education University and Research.

Data availability

Most data are described in the paper.

Acknowledgements

The work presented in this paper was performed in the frame of the EU ELSMOR project. This project received funding from the Euratom research and training programme 2019–2020 under grant agreement number 847553. The research work of Ing. Alessandro De Angelis was supported by the Ministry of University and Research (MUR) as part of the PON 2014-2020 "Research and Innovation" resources – Green/ Innovation Action – DM MUR 1061/2022.

References

Albadawi, G., Wang, S., Cao, X., 2018. Numerical and experimental study of thermal stratification outside a small SMR containment vessel, 2018. Sustainability 10, 2332.

Casey, J.R., 2013. High Pressure Condensation Heat Transfer in the Evacuated Containment of a Small Modular Reactor. Oregon State University. MSc Thesis.

ELSMOR Project Website on CORDIS, Towards European Licencing of Small Modular Reactors | ELSMOR Project | Fact Sheet | H2020 | CORDIS | European Commission (europa.eu).

Equipe CATHARE 3, 2019, CATHARE 3 V2.1.0 code: User's Manual and Guidelines, DEN/DANS/DM2S/STMF/LMES/NT/2019-65660/A, 08/12/2019.

European Commission, 2018, Communication from the commission to the European Parliament, the European Council, the Council, the European Economic and Social Committee, the Committee of the Regions and the European Investment Bank – A Clean Planet for all – A European strategic long-term vision for a prosperous, modern, competitive and climate neutral economy, November 28, 2018. https://eur-lex.europa.eu/legal-content/EN/TXT/PDF/?uri=CELEX:52018DC0773&from=EN.

Fujii, T., Takeuchi, M., Fujii, M., Suzaki, K., Uehara, H., 1968. Experiments on natural convection heat transfer from the outer surface of a vertical cylinder to liquids. Int. J. Heat Mass Transfer 13, 753–787.

IAEA, 2020, Advances in small modular reactor technology developments, 2020 Edition A Supplement to: IAEA Advanced Reactors Information System (ARIS) http://aris.iaea.org, Printed by the IAEA in Austria September 2020.
Incropera, F.P., DeWitt, F.P., 1996. Fundamentals of Heat and Mass Transfer, IV ed. John Wiley & sons.
Kataoka, Y., Fokou, T., Hatamiya, S., Nakao, T., Naitoh, M., Sumida, I., 1992. Experiments on convection heat transfer along a vertical flat plate between pools with different temperatures. Nucl. Technol. 99 (3), 386–396.
Kataoka, Y., Fujii, T., Murase, M., Tominaga, K., 1994. Experimental study on heat removal characteristics for water wall type passive containment cooling system. J. Nucl. Sci. Technol. 31 (10), 1043–1052.
Kataoka, Y., Murase, M., Fujii, T., Tominaga, K., 1995. Thermal hydraulics of an external water wall type passive containment cooling system. Nucl. Technol. 111 (2), 241–250.
Lienhard, J.H., 2020. A Heat Transfer Textbook, 5th ed. Phlogiston Press Cambridge, Massachusetts, USA.
Liu, J., Niu, F., Ahmad, B., Guo, Z., Zhu, H., Tan, Z., Jin, G., 2018. Flow characteristics in the containment cooling pools of small modular reactors, 2018. Int. J. Heat Mass Transf. 133, 445–460.
Mascari, F., Vella, G., Woods, B.G., D'Auria, F., 2012. Analysis of the OSU-MASLWR Experimental Test Facility, Vol. 2012. Hindawi Publishing Corporation, Science and Technology of Nuclear Installations.
Mullin, E.M., 2015. High Pressure Condensation in an SMR Containment. Oregon State University. MSc thesis.
NIST, 2018, NIST standard reference database 23.
Simcenter, 2018, STAR-CCM+ Documentation, version 13.06.